Ultra wideband CW pumped optical supercontinuum source

Yue Song

A Thesis

in

The Department

of

Electrical and Computer Engineering

Presented in Partial Fulfillment of the Requirements
for the Degree of Master of Applied Science (Electrical and Computer Engineering) at
Concordia University
Montreal, Quebec, Canada

October 2007

Your file Votre référence
ISBN: 978-0-494-40898-8
Our file Notre référence
ISBN: 978-0-494-40898-8

ABSTRACT

Ultra wideband CW pumped optical supercontinuum source

Yue Song

Keyword: supercontinuum, ultra wide optical source, nonlinear optical effects, continuous wave pump, ring cavity laser;

Optical supercontinuum (OSC) laser source is a new generation wideband laser which has various commercial applications such as telecommunication, biomedicine, and optical sensing systems. However the high costs of current OSC laser sources generally have impeded them to be used more widely. In this thesis, we demonstrated a low-cost OSC laser source based on a continuum wave (CW) pumped Erbium/Ytterbium co-doped fiber (EYCDF) ring cavity with a 1.2 km highly nonlinear fiber (HNLF). This OSC laser source has 350nm spectral coverage, from 1550nm to 1900nm in wavelength. This is the first CW pumped OSC that generates continuum spectrum above 1750nm. The wide spectral coverage in the long wavelength range allows more advanced utilization of OSC sources.

In this thesis, the evolution mechanism of the CW pumped OSC is discussed. The analysis of the results shows that self-phase modulation (SPM), and stimulated Raman scattering (SRS) dominate the evolution of OSC. Therefore, the evolution pattern is different to those of previous CW pumped OSCs where the modulation instability (MI) and SRS effects, or purely SRS effect dominate OSC generation. In addition, the experimental results suggest that the OSC generated by this evolution pattern has high flatness, which is caused by two reasons. Firstly, the intense SRS effect suppresses the MI effect, which could induce spectral vibration. Secondly, SPM induced spectrum broadening produce a smooth spectrum. The intense SPM and SRS effect are benefited from the ring-cavity structure which effectively increases the effective length of nonlinear fiber.

Acknowledgements

This thesis could not be finished without the help and support of many people who are gratefully acknowledged here.

At the very first, I am honored to express my deepest gratitude to my supervisor, Professor John Xiupu Zhang, with whose guidance I could work out this thesis. His guidance and help at crucial time help me obtain the final results.

I am also grateful to my co-supervisor, Dr. ZhenGuo Lu who is with Institute of Microstructural Sciences (IMS), National Research Council (NRC). He provided equipments required for my experiment and gave me many pieces of valuable advices.

The author also wants to extend his thanks to Dr. Jiaren Liu who is with IMS-NRC and has given many directions and suggestions on experimental method as well.

At last, I should express my thanks to IMS where I was permitted to complete this work.

TABLE OF CONTENTS

LIST OF FIGURES

LIST OF TABLES

ACRONYMS

ASE	amplified spontaneous emission
CW	continuous wave
DSF	dispersion shift fiber
DWDM	dense wavelength division multiplexing
EYCDF	Er/Yb co-doped fiber
FWM	four wave mixing
GVD	group velocity dispersion
HNLF	highly nonlinear fiber
MFD	mode field diameters
MI	modulation instability
NLS	non-linear Schrödinger
OCDMA	optical code division multiple-access
OCT	optical coherent tomography
OSA	optical spectrum analyzer
OSC	optical supercontinuum
PCE	power conversion efficiency
PCF	photonic crystal fiber
SLED	superluminescent light-emitting diode
SMF	single mode fiber
SNR	signal-to-noise ratio
SPM	self-phase modulation
SRS	stimulated Raman scattering
TDM	time-division multiplexing
THz	Trillion Hertz
ZDW	Zero-dispersion wavelength

Chapter 1 Introduction

1.1. Organization of the thesis

In Chapter one, the background, the general principle of optical supercontinuum (OSC) and the theories of nonlinear optical effects related to OSC generation are introduced. Then, previous researches on OSC are reviewed. Finally, the motivation of this work is given.

In Chapter two, a low-cost OSC source is proposed. The principles of this OSC source and theoretical analysis are given.

In Chapter three, the setup of the experiment is introduced. The evolution of and continuum-wave pumped OSC and experiment result will be analyzed.

In chapter four, discussions and conclusions are made.

1.2. Introduction of optical supercontinuum source

1.2.1 Wideband optical sources

Wideband optical sources are becoming more and more important for various applications, such as telecommunication, navigation system, biomedicine and metrology. The wide bandwidths of these sources allow high performances to be realized in these applications such as high resolution for detecting cells or molecules in biomedicine [1] and high capacity in communication system [2].

If only the bandwidth is considered, the best wideband optical sources are common lamps with a bandwidth of hundreds nanometers or even the sun, whose bandwidth is thousands of nanometers wide (Figure 1-1). However, these light sources obviously cannot be used in these applications because they do not meet other requirements, such as low power coupling efficiency, uneven spectrum and low coherence. On the other hand, the wideband lasers can solve these issues, because they have relatively high power coupling efficiencies, even spectra and high coherences. However, the bandwidths of traditional wideband lasers are usually limited at about tens of nanometers. For example, a typical superluminescent light-emitting diode (SLED) and amplified spontaneous emission (ASE) optical source have only about 50nm bandwidth. Figure 1-1 illustrates the spectra of the sun, SLED laser and incandescent lamp. The bandwidths of the sun and an incandescent lamp roughly are 2250nm and 350nm respectively. The bandwidth of a SLED laser is much smaller than that of non-coherence optical sources.

Therefore, all of these optical sources cannot fully satisfy the requirements of those advanced applications mentioned in the above. Based on this situation, many researches have been and still are focusing on finding a laser-like optical source with a bandwidth as wide as possible. In this study, the optical supercontinuum based light source may provide an answer to this question.

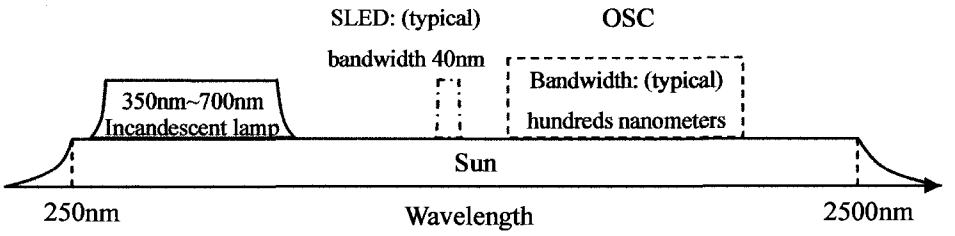

Figure 1-1 Scheme of spectra of four types of wideband light sources.

1.2.2 Optical supercontinuum source

OSC sources have attracted much attention in recent years and are being increasingly used as advanced optical sources for non-illuminating purposes in applications such as optical communication, optics gyros and optical coherent tomography (OCT). Supercontinuum is an optical phenomenon in which the spectrum of laser-like beam has an extra wide coverage of hundreds of nanometers. An OSC based optical source is a new generation of wideband laser source which has not only the high performances of other lasers but also the ultra wide bandwidth as the normal lamps (Figure 1-1).

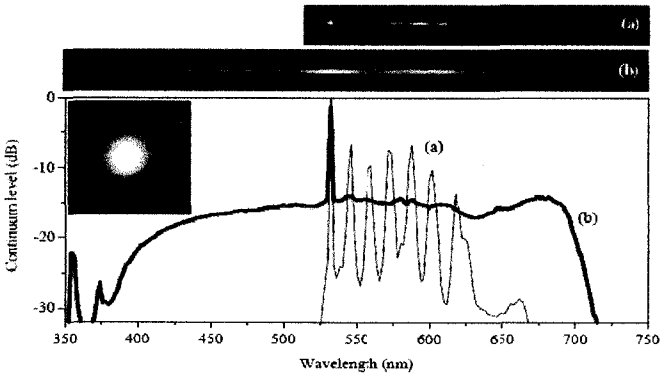

Figure 1-2 An example of OSC spectrum (source [28])

Figure 1-2 shows a white light OSC spectrum which is represented by a dark black line in this figure [28]. The spectral coverage of the OSC approaches 300nm, from

400nm to 700nm. The spectral width of this OSC is several times of that of traditional wideband lasers.

Features of OSC optical source

OSC optical sources have four major features: ultra wide bandwidth, short coherence length, high spatial coherence and flexible spectral-coverage range.

1. Ultra wide bandwidth

The bandwidths of OSC sources are usually as wide as hundreds nanometers. The wide bandwidths of OSC allow high performances to be achieved in various applications especially in the next generation of optical transmission system, in which OSC has been successfully applied in generating high-bit-rate comb of signal for high capacity long-haul systems and short pulse generation for ultra-high bit rate time-division multiplexing (TDM) systems [2]. For example, in dense wavelength-division multiplexing (DWDM) system in optical communication, the ultra wide OSC spectrum allows DWDM to obtain high system capacity [3-5]. Using an OSC source which has a bandwidth merely 80nm, an experiment in 2005 has demonstrated a 1000 channels × 2.6Gbit/s ultra-dense WDM [5]. Such a DWDM with so many dense channels benefits from OSC that easily generates well-managed multiple optical carriers because of the continuum and ultra wide bandwidth. For similar reasons, OSC sources are also used as the broadband sources of optical code-division multiple-access (OCDMA) [6].

2. Short coherence length

Two beams generated by same source can generate interference to each other in a certain propagating distance, but not beyond it. This distance is the coherence length of the beams generated by this source. Coherence length is related to the bandwidth of the beam. The wider the bandwidth of the beam is, the shorter the coherence length of the beam is. Thus, OSC beams usually have very short coherence length, because of their ultra wide bandwidth. The short coherence length feature of OSC can increase the precision and sensitivity of a fiber optic gyro or a fiber sensor in navigation systems, the resolution of OCT in medical diagnoses, and the accuracy of interferometric system in optical metrology. For example, in an experiment conducted in 2006, an OSC source with a bandwidth from 1200nm to 1550nm was successfully applied in obtaining an ultra-high-speed OCT with an axial resolution of 8μm[7]. For the OCT using conventional wideband laser, such as SLEDs, whose bandwidths is less than 100nm, the typical axial resolution cannot reach the level lower than 10μm [7].

3. High spatial coherence

Unlike conventional non-coherent white-light sources, the OSC source has high spatial coherence. In other words, like other lasers, the beam of an OSC source can be collimated into a tiny, diffraction-limited spot despite its extremely wide bandwidth [8, 9]. High spatial coherence is very useful in imaging system [1]. For example, in three-dimension surface scanning, the spot area and coherence distance of the scanning light are key parameters to the resolution of imaging. The smaller the scanning light spot is and the shorter the coherence short of the scanning light is, the higher the

resolution of the imaging. The ultra high spatial coherence and short coherence distance of OSC beam make it possible generate a nearly perfect temporally incoherent point light source.

4. Flexible spectral-coverage range

Based on different designs of OSC sources, spectra of these sources can cover the different spectral parts from visible to infrared field. The flexible spectral-coverage range enables OSC sources to be used in more applications with different spectra requirements. On the other hand, the traditional wideband lasers have more limitation in wavelength ranges.

1.3. Principle of OSC generation

Optical supercontinuum, as an optical phenomenon, is based on intense nonlinear optical effects. When a narrow-band beam with high power propagates through a medium (e.g. optical fiber), various nonlinear optical effects are generated in the medium. All of these nonlinear effects are capable of generating new frequency components, resulting in broadening the narrow spectrum of original beam into a wide continuum spectrum[10], called optical supercontinuum. Thus, the generation of OSC is a result of the combination of multiple nonlinear optical effects.

In the next section, the major nonlinear effects, which are self-phase modulation (SPM), stimulated Raman scattering (SRS), four-wave mixing (FWM) and modulation instability (MI), will be introduced.

1.4. Nonlinear optical effects

To understand the nonlinear effects more easily, some predisposing factors such as chromatic dispersions of optical fibers should be introduced firstly.

1.4.1 Chromatic dispersion

Definition of chromatic dispersion

Chromatic dispersion is one of characteristic parameters of optical fiber. When a beam propagates through a fiber, the medium (optical fiber) produces response to electromagnetic field of the beam. In other words, the electrical polarities of molecules in the medium change with the varying electromagnetic field of the beam. In general, the medium response depends on the optical frequency. This property is referred to as the chromatic dispersion [10]. The changed polarizations of molecules induce the refractive index of medium to be changed. As a result, when they propagate in same medium, the beams with different frequencies will experience different refractive indexes which will cause these beams to travel at different speed. In other words, the frequency-dependent chromatic dispersion can cause different frequency components to travel at different speeds in a fiber.

There are different types of chromatic dispersion, which include intermodal dispersion, high-order dispersions, and group velocity dispersion (GVD). When studying nonlinear optical effects, one needs to consider GVD as the main chromatic

dispersion in most cases because the intermodal dispersion is extinguished when a single-mode fiber is used, and, comparing to GVD, the high order dispersion is small enough to be neglected in most cases.

GVD causes envelops of optical signal to move at different velocities called group velocity. GVD significantly affects many important nonlinear effects such as SPM and FWM.

Zero-dispersion wavelength, normal dispersion and anomalous dispersion

Zero-dispersion wavelength (ZDW) is the wavelength at which the GVD is zero.

GVD consists of material dispersion and waveguide dispersion. When material dispersion and waveguide dispersion are canceled each other, the GVD is zero. Figure 1-2 shows the dispersion profile of a standard single mode fiber whose ZWD is 1.3 μm.

Here, two parameters related to GVD are brought up firstly. The two parameters are GVD parameter β_2 which is commonly used in calculations, and the dispersion parameter D which is normally used by industries to represent the dispersion profile of a fiber. The relationship between β_2 and D is:

$$D = -\frac{2\pi C}{\lambda^2}\beta_2 \tag{1.1}$$

GVD parameter β_2 and dispersion parameter D have opposite sign.

In Figure 1-3, the positive dispersion D ($\beta_2<0$) is called anomalous dispersion, whereas the negative dispersion D ($\beta_2>0$) is called normal dispersion. The wavelength where D=0 ($\beta_2=0$) is the ZDW.

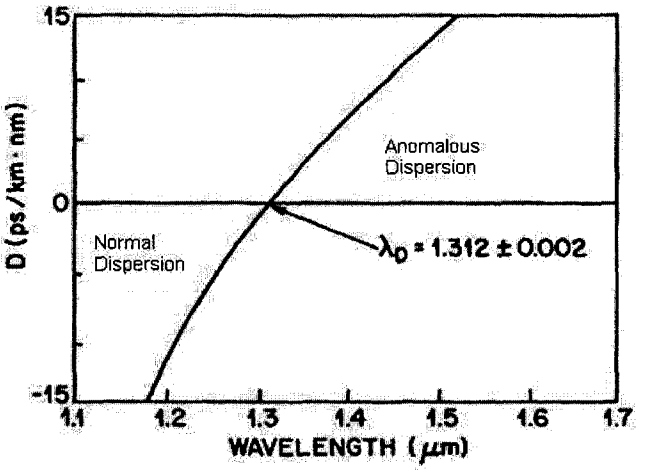

Figure 1-3 Dispersion parameter curve of a single mode fiber (source [11]).

Flat dispersion and dispersion shifted fibers

Flat dispersion means that the absolute value of the slope of a dispersion curve is relatively small. Figure 1-4 shows the profiles of dispersions of three different fibers: a standard fiber, a dispersion flattened fiber, and a dispersion shift fiber (DSF). In Figure 1-4, the dispersion flattened fiber has two ZDW and has flat dispersion between the two ZDWs. A DSF fiber is a standard fiber whose ZDW shifted from 1.3μm to the vicinity of 1.55μm. In OSC generation, flat dispersion is thought to be related to the bandwidth and flatness of the OSC spectrum [12].

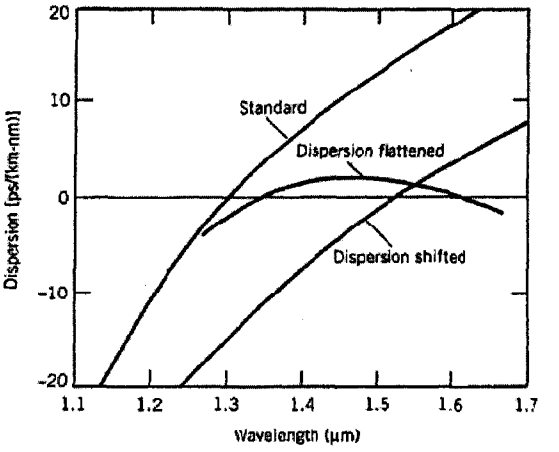

Figure 1-4 Illustrations of the dispersion profiles of three typical fibers (source [11])

Pulse compressing

An important dispersion effect, which is related to normal and anomalous dispersion, is the optical pulse compression. Because a pulse consists of numerous different frequency components, the frequency-dependent GVD causes these frequency components to propagate at different velocities which may then leads to the compression of the pulse.

The pulse compression occurs when a pulse is frequency chirped. A pulse is said to be chirped if its carrier frequencies change with time [11]. The parameter C is used to represent the chirp. Figure 1-5 shows the frequency chirp of a pulse when C is greater and less than zero. When $C>0$, the frequencies in leading edge of the pulse decrease (red shift) and the frequencies in trailing edge increase (blue shift); The opposite occurs when $C<0$. At the center of the pulse, the frequency shift is zero.

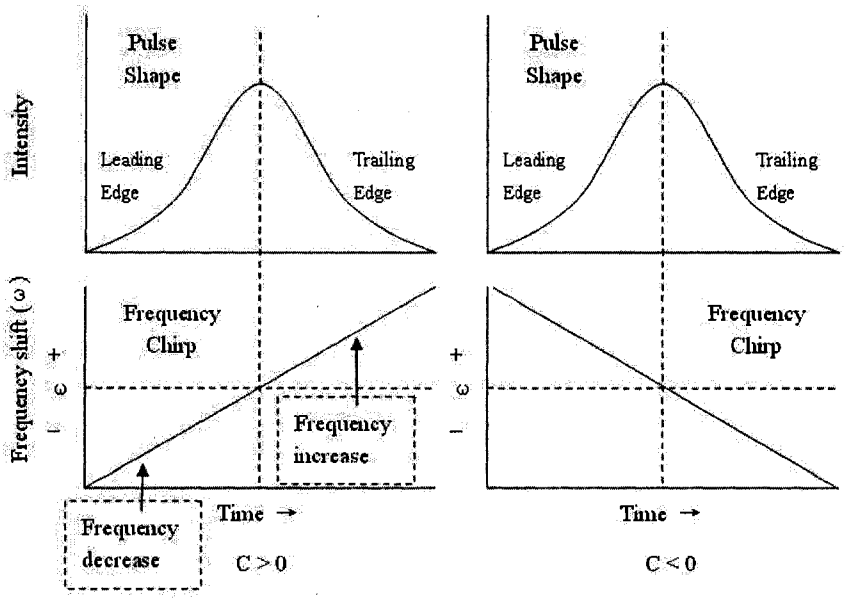

Figure 1-5 Frequency linear chirp for parameter C >0 and C<0 (source [10]).

The dispersion will cause the different frequency components to propagate at different speed. In normal dispersion region (β_2 >0, D<0), the normal dispersion causes the red components (lower frequency) to travel at a faster speed than that of the blue components (higher frequency); and oppositely, in anomalous region (β_2 <0, D>0), the blue components travel faster than red components.

Pulse compressing only happens when $\beta_2 C < 0$. For example, a pulse with positive chirp (C>0) propagating down a fiber experiences the anomalous dispersion (β_2 <0). The red-shifted components in leading edge of pulse travel slower than the blue shift components in trailing edge. As this result, the trailing edge is gradually close to the leading edge and the pulse is compressed. The pulse compress plays an important role in many of OSC generation.

1.4.2 Self phase modulation

After the introduction of chromatic dispersion, now it is time to introduce the nonlinear effects. The self phase modulation is the first to be described.

Basic concept

SPM is a phenomenon in which the phase of an optical signal shifts as the result of the interaction between the optical signal and the medium. More specifically, optical signals usually consist of multiple frequency components. These components can generate a nonlinear dispersion. The nonlinear dispersion will cause these components to propagate at different speeds, in other words, the dispersion causes the phase shift of optical signal. More specifically, the refractive index of the fiber alters with the varying optical intensity of the optical signal. The variation in the refractive index will produce a nonlinear dispersion. Furthermore, the nonlinear dispersion causes a nonlinear phase shift in the signal, and this nonlinear phase-shift phenomenon is called SPM.

SPM induced spectrum broadening

SPM induced spectrum broadening will be explained mathematically. Firstly, it is assumed that the normalized amplitude of a signal is $U(z,T)$, where z is the propagating distance of the signal, and T is the normalized time.

The nonlinear phase shift at propagation distance L is given by:

$$\phi_{NL}(L,T) = |U(0,T)|^2 (L_{eff}\gamma P_0) \tag{1.2}$$

where L_{eff} is the effective length of optical fiber, γ is the nonlinear coefficient of

the fiber. P_0 is the optical power of the signal, and

$$L_{eff} = [1 - \exp(-\alpha L)] / \alpha \tag{1.3}$$

where α and L are the loss and length of the fiber, respectively.

Equation 1.2 shows that the SPM induced phase shift is dependent on time variable, *T*. The time-dependent nonlinear phase shift implies that new frequencies are generated. The frequency difference between the new frequency and the center frequency is:

$$\delta\omega(T) = \frac{-\partial\phi_{NL}}{\partial T} == -\gamma P_0 L_{eff} \frac{\partial}{\partial T}|U(0,T)|^2 \tag{1.4}$$

According to Equation 1.4, when the wave shape $U(0,T)$ of signal is fixed, the frequency broadening depends on the nonlinear coefficient γ, signal peak power P_0, and the effective fiber length L_{eff} that is related to the fiber loss α and fiber length L. Practically, nonlinear coefficient and loss, which are physical properties of a fiber, cannot be altered. Therefore, SPM induced spectrum broadening can be only obtained by increasing the length of fiber and the optical power.

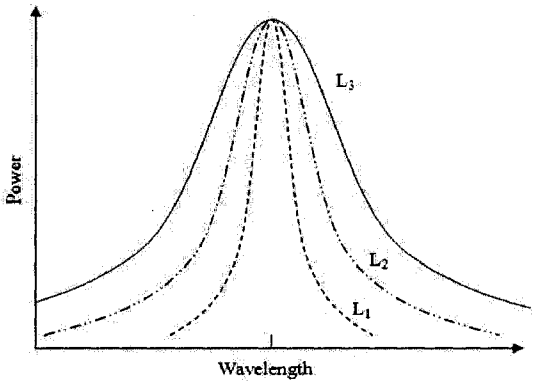

Figure 1-6 Illustration of SMP-induced spectral broadening of a CW signal for three different propagating distances, where L3>L2>L1 (source [10]).

Figure 1-6 shows a SPM induced spectrum broadening at three fiber lengths

($L_3>L_2>L_1$) when the signal is a continuous wave signal. The spectrum broadening is biggest when the fiber has longest length L_3.

Pulse compression induced by interaction between SPM and GVD

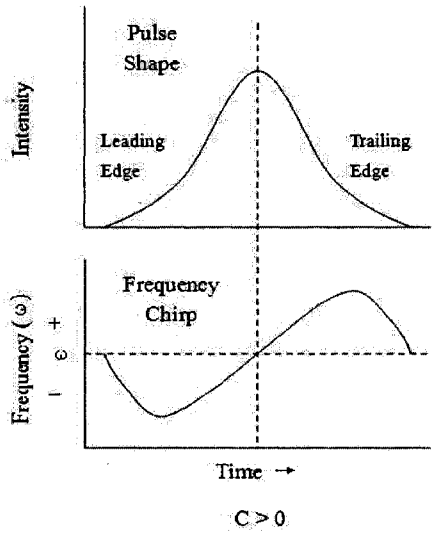

Figure 1-7 Illustration of SPM induced chirp (source [11]).

When an optical pulse produces SPM effect, SPM will impose a positive nonlinear chirp in the pulse. Figure 1-7 illustrates SPM induced chirp in a pulse where the red-shift of frequency occurs in leading edge and blue shift occurs in trailing edge. If the pulse experiences anomalous dispersion region (β_2 <0) at the same time, the condition $\beta_2 C < 0$ is satisfied and the optical pulse will be compressed (see Section 1.3.1 - pulse compressing). The pulse compressing induced by SPM and GVD was used in some experiments of OSC generation, in order to obtain high peak power of optical pulses.

1.4.3 Stimulated Raman scattering

The second nonlinear optical effect introduced here is stimulated Raman scattering (SRS).

Basic concept

When a photon is travelling in a medium, e.g. optical fiber, the photon is scattered by a molecule of the fiber and transfers a small fraction of energy to the molecule. As a result, this photon becomes a low frequency photon due to energy loss. This process is called a Raman effect. The new low-frequency component is called Stokes wave [10]. The Raman effect can produce a wide gain spectrum at the low-frequency region. The detail about Raman gain will be described later. When a weak signal co-propagates with an intense pump beam in a fiber and if the frequencies of the weak signal lie in the Raman gain spectrum of the pump beam, a stimulated emission will occur at the frequencies of the weak signal, leading energy from the pump beam to the weak signal. In the other word, the weak signal is amplified by the Raman gain. This phenomenon is referred to stimulated Raman scattering (SRS).

Raman gain spectrum

The Raman gain is represented by Raman gain coefficient g_R which is related to the cross section of spontaneous Raman scattering [10]. Figure 1-8 shows the Raman gain spectrum of a silica fiber. The width of Raman gain spectrum is about 40THz. An important feature of Raman gain in the silica fiber is that the wide gain peak is always

at 13THz away from pump frequency. The well-defined frequency is caused by the physical property of silica.

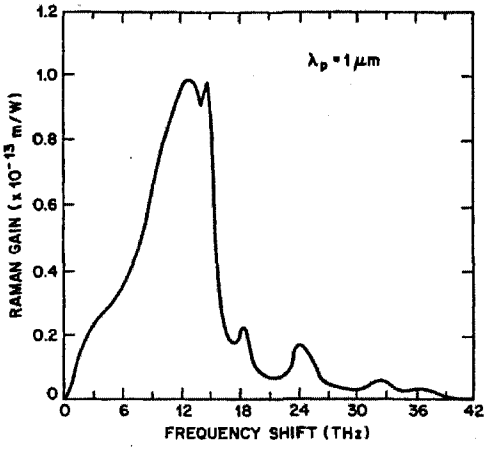

Figure 1-8 Raman gain spectrum of fuse silica (source [10])

The Raman gain can be used to amplify weak optical signals in optical communication by generating SRS effect at frequencies of the signals. When only the pump beam propagates in a fiber, the spontaneous emission noise within the gain spectrum will act like the signal, thereby amplifying these signals. Furthermore, these signal-like noise components are amplified by Raman gain and the frequency components around 13 Trillion Hertz (THz) from the pump wave grow up most rapidly.

Threshold power of SRS

The threshold power is defined as the pump power at which the power of the Stokes peak is equal to the pump power. When pump optical power exceeds the threshold power, the SRS effect can be built up. The approximate estimation of the threshold power is given by the equation:

$$P_0 \approx \frac{16 A_{eff}}{g_R L_{eff}} \tag{1.5}$$

where A_{eff} is the effective core area of fiber, the g_R is the Raman gain coefficient, and L_{eff} is the effective nonlinear length of the fiber as defined in Equation 1.3 (Section 1.4.2).

From Equation 1.5, the threshold power is mainly related to three parameters of a fiber: the effective core area, the effective nonlinear length, and the Raman gain coefficient which can be adjusted to control SRS.

Firstly, the threshold power can be changed by choosing different types of fiber with different effective core areas and Raman gain coefficients. For a single mode fiber (SMF) which has big effective core area, the threshold power could be as high as hundreds mill-watts. However, for a highly nonlinear fiber (HNLF), the threshold is reduced very much, since its effective core area is much smaller than that of a single mode fiber. Additionally, there are some fibers that have high Raman gain coefficients, which are designed to generate intense SRS effect.

Secondly, the threshold power can be changed by changing effective-nonlinear length. The effective nonlinear length, however, is related to the loss and length of a fiber. The smaller the loss is or the longer the fiber is, the longer the effective length is, and, therefore, the easier the SRS generation in the fiber.

The estimation using Equation 1.5 is based on an assumption that the polarization of the incident beam is maintained throughout whole fiber [10]. However, when the

polarization is scrambled in the fiber, the level of threshold power could be increased or even be double.

Cascaded Stokes peaks

During the process of SRS occurring, the pump beam transfers power to the Stokes wave, and the Stokes peak in spectrum keeps growing up by increasing the pump power. When the Stokes wave has a sufficient power to generate the SRS effect, a second-order Stokes peak can appear in spectrum. Furthermore, a series of higher order Stokes peaks could be obtained, if the pump power was increased further. This multiple-order Stokes peaks are called cascaded Stokes peaks. Figure 1-9 shows a spectrum of five-orders Stokes peaks when pump power is 840mW. The five-order Stokes peaks broaden the spectrum from 1.05μm to 1.45μm. The cascaded SRS effect is one of important means to broaden OSC spectrum, since it can seeds new frequency components at the frequencies far away from the pump peak.

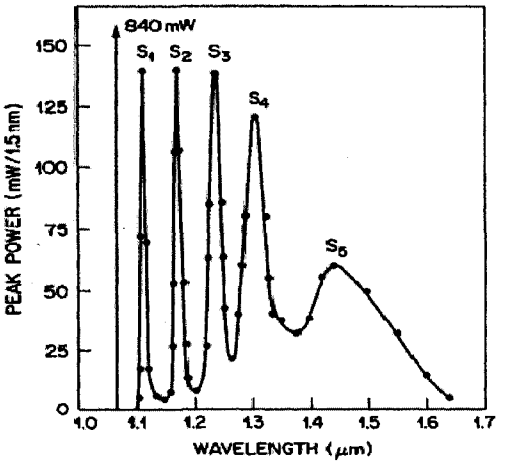

Figure 1-9 Cascaded Raman Stokes peaks, where the Stokes peaks, S1 to S5, are generated by a 1060nm pulse pump. (source [10])

1.4.4 Four wave mixing

Four-wave mixing (FWM) is the third nonlinear optical effect to be introduced here.

Basic concept

FWM effect can be simply understood as photons with one wavelength or different wavelengths being annihilated and new photons being generated at new wavelengths. During the process of generating FWM effect, net energy and momentum are conserved [10]. This process is different from SRS effect where the energy is transferred to molecules of the fiber to cause them to vibrate. In FWM effect, the new waves at long wavelengths are Stokes peaks, oppositely, the new peaks generated at short wavelengths are called anti-Stokes peaks. To produce FWM, the major condition is that these photons are approximate phase matching.

Two cases of FWM

FWM effect could occur in two cases, non-degeneration case and partial degeneration case.

1. Non-degeneration case is the situation where three pump photons at frequencies, ω_1, ω_2 and ω_3, create a new photon at ω_4. The new photon could be generated at nine possible frequencies (including when $\omega_1 \neq \omega_2 \neq \omega_3$ and $\omega_1 = \omega_2 \neq \omega_3$) . The possible frequencies are:

$$\omega_4 = \pm\omega_1 \pm \omega_2 \pm \omega_3$$

Figure 1-10 illustrates a non-degeneration case where we can see that a lot of new frequency components are generated within the spectrum. Thus, FWM effect is helpful to OSC generation, since it is highly efficient at generating large quantities of new frequencies. However, the non-degeneration FWM rarely occur since phase-matching condition of so many photons is difficult to be satisfied in most situations.

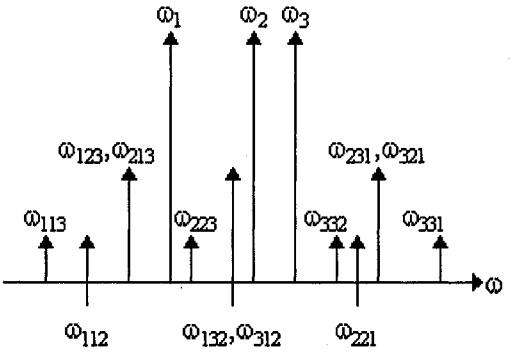

Figure 1-10 Illustration of FWM effect when three pumps co-propagate in fiber (source http://www.npl.co.uk/photonics/nonlinear/four_wave_mixing.html)

2. Partial degeneration case is that two pump photos, at ω_1, and ω_2, generate two new photons at ω_3 and ω_4. Figure 1-11 (left part) shows the partial degeneration case where ω_1 is not equal to ω_2. The frequency relationship in them is:

$$\omega_1 + \omega_2 = \omega_3 + \omega_4$$

A special case in partial degeneration FWM is that ω_1 is equal to ω_2. That means two pump photons with same frequency create two new photons. The right part in Figure 1-11 shows the special case. The frequency relationship between of them is:

$$2\omega_1 = \omega_4 + \omega_3$$

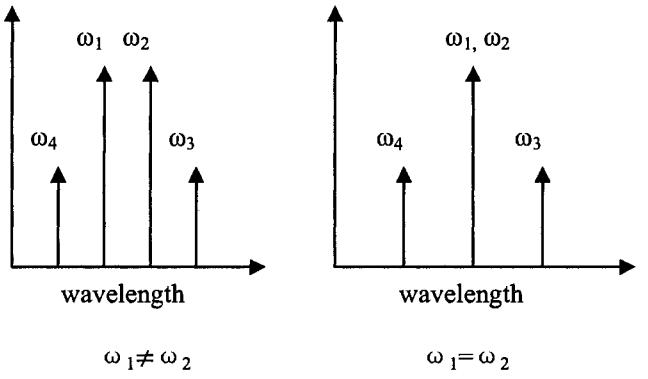

Figure 1-11 Illustration of partially degeneration FWM effect (source [11])

Comparing to the non-degeneration case, the partial degeneration case is easier to obtain, since the phase matching of less photons is easier to be achieved in this case.

Phase matching in FWM

FWM only occurs when phase-matching condition is satisfied. The phase mismatch is generally caused by a GVD with high absolute value, since GVD can cause the waves with different wavelengths to travel in different group velocities. The Δ is used to express the phase mismatch. Δ can be approximately calculated using this equation [10]:

$$\Delta = \beta_2 \Omega^2 \tag{1.6}$$

where β_2 is the GVD parameter, Ω is frequency shift, i.e. $\Omega = \omega_1 - \omega_3 = \omega_4 - \omega_2$ (assuming a partial degeneration FWM, where $\omega_3 < \omega_4$).

The smaller phase mismatch Δ is, the better phase matching is, and the more likely the FWM will occur.

According to Equation 1.6, when β_2 is zero, in other words GVD is zero, the phases of the four waves are perfectly matching. Therefore, for OSC generation, the major method to achieve phase matching is to let the wavelength of pump beam be close to the zero-dispersion wavelength (ZDW) of a fiber. The extra low GVD around ZDW is a favorable condition to achieve phase matching.

SPM effect has been also used to achieve phase matching of FWM effect in OSC generation. In this method, SPM induced nonlinear dispersion is utilized to cancel out the GVD. The FWM effect generated from SPM induced phase matching often happens in OSC generation.

1.4.5 Modulation instability

The last nonlinear optical effect to be described is modulation instability (MI).

Basic concept

The nonlinear and dispersive effects cause a nonlinear system to exhibit an instability that further leads to a modulation of the steady state. This phenomenon is referred to as modulation instability [10]. In other words, when a pump wave propagates down a fiber and experiences anomalous dispersion, the nonlinear system, which consists of pump wave and nonlinear medium, becomes unstable. Consequently, some weak perturbations, which could be noise or signals, are amplified continually in this system. In fact, MI effect causes the breakup of the pump wave into ultrashort

pulses train. Because of this feature, MI is interested by many researchers in OSC generation. This will be further described.

Gain spectrum of MI

The MI effect can produce a symmetric gain spectrum about the center frequency of the pump wave. When noise within the gain spectrum is amplified by the gain spectrum, two side lobes are formed and are symmetric about the center frequency of the continuous wave (Figure 1-12). The frequency shift Ω of the gain spectral peak is given by [10]:

$$\Omega = \pm\left(\frac{2\gamma P_0}{|\beta_2|}\right)^{1/2} \tag{1.7}$$

where γ is the nonlinear coefficient, P_0 is the pump power and β_2 is the GVD parameter:

According to Equation 1.7, the nonlinear coefficient and incident power have positive impact on MI induced frequency shift, whereas the value of GVD has a negative impact. Thus, to generate OSC, the wavelength of pump wave is chosen to lie at anomalous dispersion region and is close to ZDW. The anomalous dispersion induces the MI effect to occur. Low dispersion around ZDW can enhance the MI effect.

An important feature of MI is the red-shift and blue-shift of the two side lobes. Figure 1-12 shows the gain spectrum of MI in three different pump power levels P_1, P_2 and P_3 ($P_1<P_2<P_3$). We can see that the low-frequency side lobe exhibits red-shift and the high-frequency side lobe exhibits blue-shift as the pump power is increased.

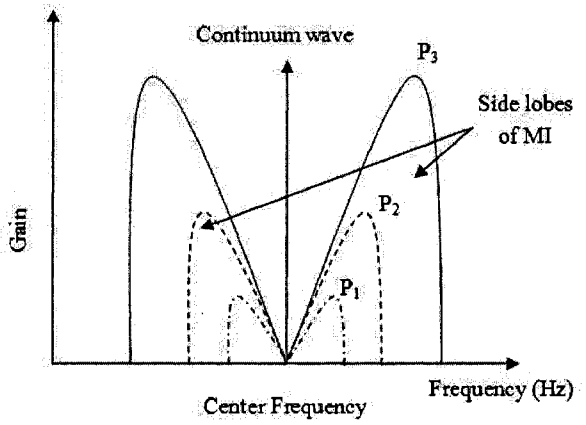

Figure 1-12 Illustration of MI gain spectrum in three different pump levels, where P3>P2>P1 (source [10]).

1.5. Review of researches in OSC

After introduction of the major nonlinear effects in OSC generation, now let us take a look at recent works that have been done on OSC. The optical supercontinuum phenomenon was first observed in 1970 by Alfano and Shapiro[13, 14]. Although a number of researches on OSC have been carried out since early 1990's, the mechanism of OSC generation still cannot be completely understood because numerous nonlinear optical effects, such as self phase modulation (SPM), four wave mixing (FWM), stimulated Raman scattering (SRS), and modulation instability (MI) have been implicated in this process, and these nonlinear effects interact with each other, in different extents making analysis of this process so complicated. Thus, researches on OSC have been focusing on generating high quality OSC by different methods rather than explaining the intrinsic mechanisms. However through these experiments, the

mechanism of OSC generation has been revealed gradually.

In an OSC source, pump laser is an important component since different pump lasers generate OSCs in different ways and thus have different results. According to the types of pump laser, the OSC sources obtained in past researches can be classified as ultrashort pulse pumped and continuous wave pumped. The ultrashort-pulse pump has optical pulses with picoseconds duration time and kilowatts peak power. The continuous wave pump has continuous optical wave which has low peak power, in general only several watts. Besides the pump laser, the nonlinear fiber is another key component in OSC generation since it is directly related to how and which nonlinear effects are generated and to what extent. There are two types of nonlinear fibers, highly nonlinear fiber (HNLF) and photonic crystal fiber (PCF) that have been used in experiments of OSC generation. In this section, these nonlinear fibers will be introduced firstly. After that, the introductions of CW pumped and ultrashort pulse pumped OSC sources will be given.

1.5.1 Nonlinear optical fibers

Nonlinear fibers are designed to produce intense nonlinear optical effects. Nonlinear optical effects occur when an intense beam propagates in a medium. The strong electromagnetic field of beam causes the polarizations of electric dipoles in the medium to nonlinearly vary with the power of beam. Furthermore, the varying polarizations of electric dipoles induce the nonlinear optical effects to occur. The

higher the optical power through per unit cross-section area of a fiber is, the stronger the nonlinear effects are. Thus, a basic principle of nonlinear fibers is to confine the optical intensity to small cross-section area of the fiber. The capability that a fiber generates nonlinear optical effects is usually represented by nonlinear coefficient γ in calculations.

Highly nonlinear fiber (HNLF)

Highly nonlinear fibers (HNLFs) obtain high nonlinear coefficient through changing the refractive index in the core or cladding of fiber. By this way, all optical beams are confined to much smaller core area than that in normal fibers, and the optical power density in the core of HNLF is thus higher than that in normal fibers. Therefore, HNLFs have a much higher nonlinear coefficients than normal optical fiber such as standard single mode fiber, whose typical value of nonlinear coefficient is $1.46(km \cdot W)^{-1}$ [15], whereas, the value of a HNLF is above $10(km \cdot W)^{-1}$. Some special HNLFs can even have a nonlinear coefficient of $1000(km \cdot W)^{-1}$.

Photonic crystal fiber (PCF)

PCF is a type of micro-structure fiber that has regularly arranged micro air-holes in the core area of the fiber. Figure 1-13 shows a cross section picture of a PCF. The diameters of these holes are usually less than 1 micrometer. When a light propagates in PCF, the light is confined to a very narrow core area by the internal reflective effect or

a photonic band-gap effect. All optical power is focused into the small area which gives rise to a high energy concentrated region to allow nonlinear effects to occur easily. The nonlinear coefficient of a PCF can be as high as 80 $(km \cdot W)^{-1}$ (NL–2.3–790, manufactured by Crystal Fiber, where ZDW is 790±5nm) [46].

Comparing with HNLF, PCF has obvious advantages on the dispersion characteristic. The dispersion profile of a PCF can be simply changed by adjusting the arrangement or the diameter of these air-holes. By this way, the ZDW of PCF can be shifted to as low as 1000nm where ZDW of HNLF cannot be shifted to[16]. Additionally, very wide flat-dispersion region can be achieved in PCF. In some PCF, the width of flat dispersion can be above 100nm. Such a wide flat dispersion is hard to be obtained in HNLF. Wide and flat dispersion is helpful to obtain wide and flat OSC spectrum [12]. Thus, many experiments used dispersion-flatten PCF to generate OSC [17-19].

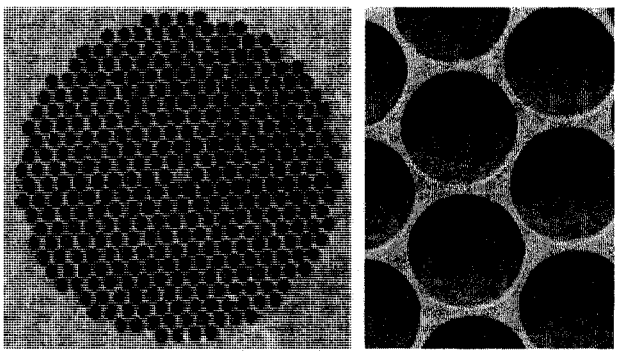

Figure 1-13 Cross section picture of a PCF made by US Naval Research Laboratory. (source http://www.nrl.navy.mil/techtransfer/fs.php?fs_id=97)

Because of the advantages of PCF on dispersion, it becomes quite suitable for generating OSC. Thus, PCFs were used in most of ultrashort pulse pumped OSC, and several broadest OSCs were generated in PCFs. However, the prices of PCFs are usually several times to those of HNLF, thus increasing the cost and limiting its usage in industrial products. Additionally, HNLF has relatively low loss (per kilo-meter) and low splicing loss with other fibers, whereas PCF usually has quite high loss. For example, the PCF, NL–2.3–790 (manufactured by Crystal Fiber), has 90dB/km loss at ZDW [46], in contrast that the loss of a HNLF is usually less than 1 dB/km. Furthermore, the high loss of PCF causes nonlinear effects to be suppressed in long PCF. Additionally, the complex structure of PCF makes the PCF so difficult to be spliced with other fiber. As a result, the splicing loss of PCF is usually much higher than that of HNLF.

Table 1 gives a comparison between HNLF and PCF. According to these advantages and disadvantages of PCF and HNLF, PCF is more suitable to be used in ultrashort pulse pumped OSC since high peak power of optical pulse allows short PCF to be used. The problems, high loss and high cost (per kilometer), can be partially avoided when short PCF is used. On the other hand, HNLFs are more suitable for CW pumped OSC generation, since low peak power of continuous wave requires long fiber. The low loss and low cost (per kilometer) make HNLF be the better choice for CW pumped OSC sources.

Table 1 Comparison of PCF and HNLF

	PCF	HNLF
Advantages	■ High nonlinear coefficient (could be much higher that $30\,(km \cdot W)^{-1}$) ■ Good dispersion property (flat dispersion, flexible ZDW)	■ Low loss (could be lower than 1dB/km) ■ Cheap ■ Low splicing loss
Disadvantages	■ High loss (per kilo-meter) ■ Expensive ■ High splicing loss	■ ZDW can be shifted only in a narrow spectral range

1.5.2 Ultrashort pulse pumped OSC

Traditionally, OSC is generated by pumping a train of ultrashort optical pulses into a nonlinear fiber. Ultrashort optical pulse has high peak power of kilowatts. The high peak power can be used easily to generate intense nonlinear effects in short fiber because intensities of nonlinear effects depend on optical power and fiber length. High optical power can compensate for short fiber. Using short fiber in OSC source can effectively reduce the size of source.

Ultrashort pulse pumped OSC can be classified by the types of dispersion at which pump beam propagates. Two major types of dispersions are the normal dispersion and the anomalous dispersion.

1. Propagating in anomalous dispersion region

Most of experiments of ultrashort pulse pumped OSC set the pump wavelength in anomalous region and near ZDW, since very wide OSC could be obtained by this way.

Choosing pump wavelength at anomalous dispersion and close to ZDW has three advantages.

Firstly, Pumping pulse in anomalous dispersion region can generate MI effect. Some simulations and experiments have shown that OSC generation is determined by MI effect [20, 21] because MI effect interacting with anomalous dispersion can produce optical soliton, a special ultrashort optical pulse. The FWM effect produced by solitons and self-frequency-shift of solitons are thought to be the major mechanisms of OSC generation [20].

Secondly, anomalous dispersion can be used to compress the optical pulse. Anomalous dispersion interacting with SPM effect can compress pump pulse to narrower optical pulse (Section 1.4.2). Comparing to the original pump optical pulse, the compressed pulse has higher peak power which can generate richer nonlinear effects and broaden the spectrum of OSC greatly [16, 21-23].

Finally, making the center frequency of optical pulse close to ZDW is advantageous for FWM to occur, since the extremely low GVD around ZDW enables the phase matching condition of FWM effect to be easily achieved. Additionally, the low GVD is favorable condition to enhance the MI effect. By the same reasons, in CW pumped OSC, the pump wavelength was also chosen at the anomalous dispersion side of ZDWs.

To summarize, when the pump pulses propagate in anomalous dispersions region, MI effect together with FWM and SRS can produce very wide OSC. However, the spectrum of OSC often shows intense spectral vibration and noise which are caused by

pulse break-up and the MI effect [24, 25]. To avoid this problem, pumping pulses in normal dispersion region was used in some ultrashort pulse pumped OSC sources.

2. Propagating in normal dispersion region

Although broadening OSC in anomalous dispersion region is advantageous for obtaining wide OSC spectrum, the spectral variation and noise of OSC produced by this way cause OSC sources to be difficulty to be used in some applications. Some experiments showed that the normal dispersion can improve the flatness of OSC spectrum [25-28] since the MI effect rarely occurs at normal dispersion region. Additionally, in normal dispersion region, the spectrum broadening is dominated by SPM and SRS which induce smooth and stable OSC spectrum. Figure 1-14 shows four ultrashort pulse pumped OSC spectra at the same level of pump power. These spectra are generated by injecting four optical pulses with different center frequencies into a PCF [29]. The PCF has ZDW at 900nm and normal dispersion of below 900nm. The center wavelengths of the four pulses are chosen at 800nm, 825nm, 850nm and 875nm. We can find that the spectrum whose pump wavelength is at 800nm is smoother than the others, since SPM and SRS dominate the spectrum broadening. When the pump wavelength moves close to ZDW, the spectra become vibrating more and more. The spectral vibration is caused by the broadening of the partial spectrum into anomalous dispersion region where MI induced break-up of pulse which causes more serious spectral vibration in anomalous dispersion region [29]. This phenomenon proved that

OSC broadened in normal dispersion region is smoother than that in anomalous dispersion region.

Additionally, from Figure 1-14, we also can find that OSC spectrum is becoming wider while the pump wavelength moves to ZDW. It shows that richer nonlinear effects occur as pump wavelength is closer to ZDW. This phenomenon implies that pumping pulse at anomalous dispersion and close to ZDW is advantageous to spectrum broadening.

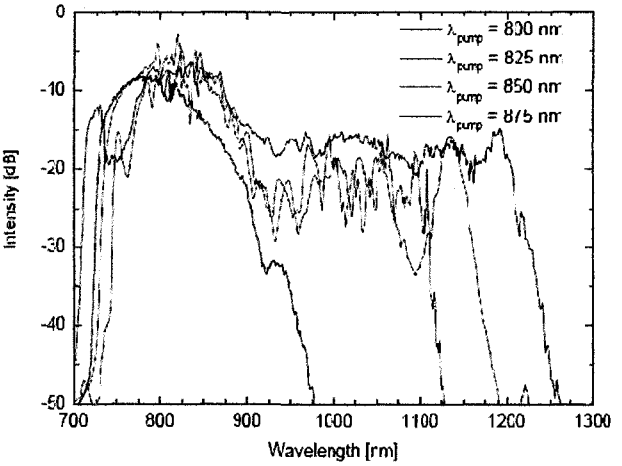

Figure 1-14 Ultrashort pulse pumped OSCs formed at different pump wavelengths. (source [29]).

Although the bandwidths of OSCs generated in normal dispersion region were usually narrower than those generated in anomalous dispersion region, the qualities of spectra are much higher. Thus, these OSCs are more suitable for industrial applications.

1.5.3 Continuous wave pumped OSC

The continuous-wave (CW) pumped OSC source generates OSC beam by pumping CW beam into a nonlinear medium. Currently ultrashort optical pulse source is more

widely used as the pump source since optical pulse with high peak power has advantage on generating nonlinear effects. Comparing to ultrashort optical pulse, CW beam has much lower peak power which is disadvantage to produce rich nonlinear effects. Thus, CW pump had never been used for OSC generation until 2003, two groups have demonstrated that CW pump can be used to produce OSC in HNLF and PCF [30, 31].

The evolution mechanism of CW pumped OSC, however, has never been consistently concluded. Since then, experiments of CW pumped OSC have showed different patterns of evolution. These patterns can be roughly classified into three types, MI and SRS dominated, purely SRS dominated and FWM dominated OSC evolution.

MI and SRS dominated evolution

In most of CW pumped OSC experiments, the OSC generation is dominated by MI and SRS effects. In these experiments, the pump wavelength is located at the anomalous dispersion region and at vicinity of ZDW. The continuous wave propagating in anomalous dispersion region produces MI effect which causes the spectral peak of CW beam to be broadened [30, 32-35]. Meanwhile, the CW pump beam generates SRS effect which dominates the spectrum broadening toward long-wavelength region. Figure 1-15 shows a typical CW pumped OSC in which the evolution is dominated by MI and SRS [36]. In the beginning, two side lobes of MI effect appear around pump peak when pump power is 0.42W. Then the pump peak is broadened by MI effect with

increase of pump power. When pump power is above 1.062W, the SRS generates a spectral peak around 1650nm. Meanwhile, the long-wavelength side lobe of MI falls in the gain spectrum of SRS and is amplified by Raman gain to form continuum spectrum. Finally, SRS and MI interact to generate the OSC. It should be mentioned that the high spectrum level between 1700nm and 1750nm is the noise spectrum due to optical spectrum analyzer when pump power is 0.42W.

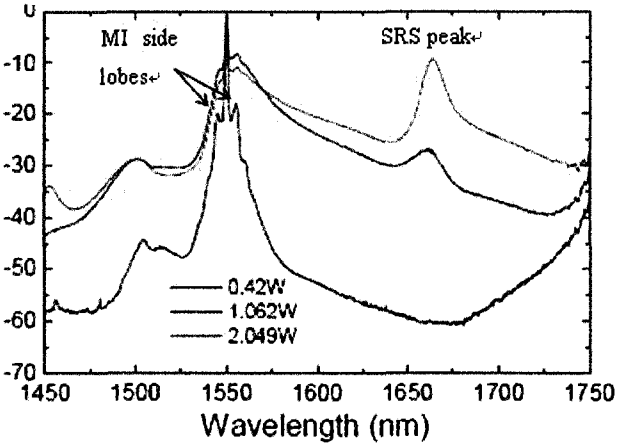

Figure 1-15 A typical CW pumped OSC dominated by MI and SRS (source [36])

In another CW pumped OSC which was obtained in an experiment conducted by Ju Han Lee, et al., [46], MI and SRS dominated evolution can be observed as well. Figure 1-16 shows the evolution of this OSC. In this experiment, the wavelength of the pump wave is at 1568nm. MI induced soliton and SRS effect broaden the spectrum toward long-wavelength direction (>1568nm). Meanwhile, it can be found that MI effect and FWM effect broaden the spectrum toward short-wavelength direction (<1568nm) greatly. The spectrum coverage of this OSC approaches 470nm.

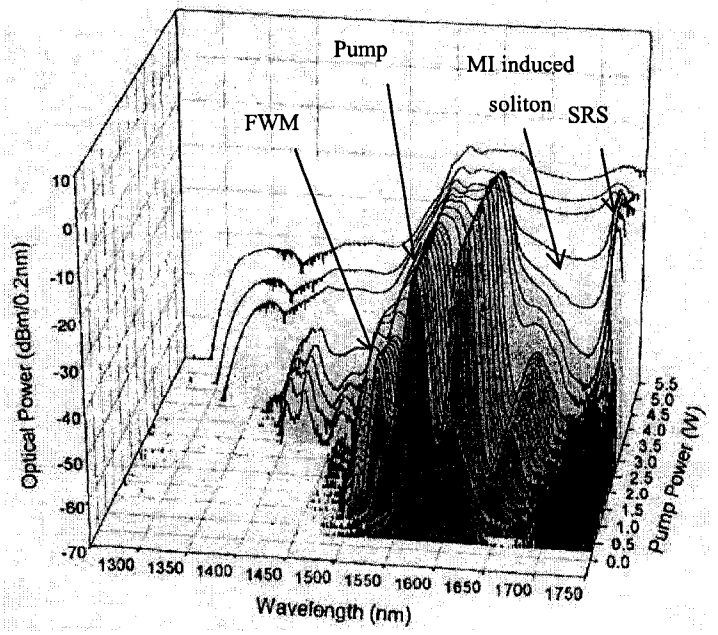

Figure 1-16 Evolution of a MI and SRS dominated CW pumped OSC (source [46])

In these experiments where MI and SRS dominated the spectrum broadening, long fibers were usually used to enhance the SRS effect. The lengths of fiber were usually above 3km. The long fiber is disadvantageous in that it leads a large size of the OSC source.

Purely SRS dominated evolution

A few experiments showed a totally different OSC generation pattern where the evolution of OSC is purely dominated by SRS effect [31, 37]. In these experiments, the spectrum broadening mainly depends on cascaded Raman Stokes peaks which require high pump power. For instance, in one of the experiments done by Avdokhin et al., [31], the pump power is as high as 100W.

A common characteristic of these experiments is that these OSCs were generated in

high anomalous dispersion region, for example the dispersion parameter D in Avdokhin's experiment is as high as 45 $ps/(nm \cdot km)$. The high dispersion deterred MI occurring in these experiments. Figure 1-17 shows an SRS dominated CW pumped OSC, where there is no obvious MI effect. A problem caused by high dispersion is a large amount of spectral vibration since the high dispersion induces intense dispersion waves [35].

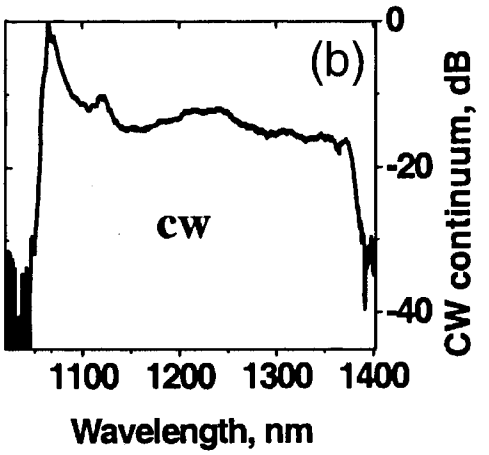

Figure 1-17 CW pumped OSC purely dominated by SRS (source [31])

3. FWM dominated evolution

Obtaining OSC by enhancing FWM in serially connected dispersion-shifted fibers (DSFs) which have different ZDWs was demonstrated in an experiment conducted by Li, et al., [38]. By carefully choosing the ZDW of each fiber, new spectral peak generated by FWM in the previous DSF will fall in the ZDW of the next DSF. FWM can occur at these ZDWs since phase matching is easy to be satisfied. As a result, the new spectral peak in the next DSF can generate more FWM wave and produces two

new spectral peaks. Finally, the OSC is formed by cascaded FWM effect.

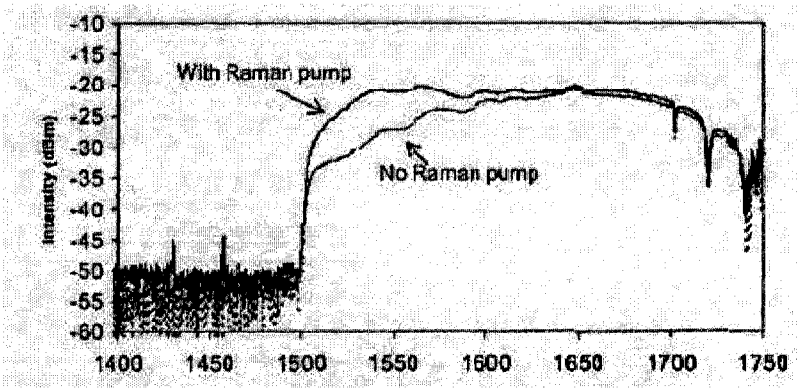

Figure 1-18 OSC generated in cascaded DSFs, where FWM dominated the spectrum broadening (source [38])

Figure 1-18 shows the result of this experiment. The 15dB bandwidth is 268nm. The spectrum is relative flat when a Raman pump is used. To obtain such a result, only a pump power 1.96W and a 2-km fiber were used in this experiment. However, a defect of this method is that there is high requirement for the ZDW of DSF. It is hard to find so many DSFs with proper ZDWs.

Characteristics of CW pumped OSC

1. Long fiber or high pump power

Long fiber is usually required in CW pumped OSC. Since low peak power of continuous wave reduces the intensity of nonlinear effects, long propagation distance is used to compensate for the low peak power. Alternatively in some experiments, to reduce the length of fiber, more high pump power was used [31, 37].

2. SRS dominated evolution:

Till now, in most of experiments of CW pumped OSC, SRS effect has dominated the

spectrum broadening. This phenomenon is because long fibers were used in CW pumped OSCs. Since SRS effect occurs along entire fiber, SRS effect in a long fiber is stronger than that in a short fiber.

1.5.4 Comparison of CW pumped and ultrashort pulse pumped OSC

Most of experiments on OSC generation use ultrashort pulse as the pump source, therefore relatively mature technologies were developed in this way. Comparing to ultrashort pulse pumped OSC, the studies of CW pumped OSC have been carried out for only several years. The bandwidths of CW pumped OSCs has not increased significantly, thus being narrower than those of ultrashort pulse pumped OSC. However, experiments of CW pumped OSC have already proved its advantages over ultrashort pulse pumped OSC.

1. Potential low cost:

Cost of ultrashort pulse pumped OSC is high. A major reason causing this high cost is that ultrashort pulse sources are usually in the range of tens of thousands of dollars. On the other hand, devices in CW pumped OSC source are usually relative less cost. For instance, a high power CW pump only costs hundreds of dollars.

2. High spectral power density:

Continuous wave pump laser has much higher average output power than that of ultrashort pulse laser. As a result, the spectral power density usually is quite higher in CW pumped sources. The high spectral power density is quite important for industrial

applications since it can increase the signal-to-noise ratio (SNR) of the applied equipment. A high SNR allows high performances, such as sensitivity or accuracy, to be achieved in applied equipments.

3. High stability and reliability :

CW pumped OSC sources have high reliability and stability partially due to its simple structure. Additionally, the CW pump lasers have been proven to be stably operated under an unfavorable environment such as extreme temperatures and humidities, conferring the stability and reliability of OSC source as well.

1.6. Motivation and Objective

OSC source has great potential to be used in various cutting-edge applications; moreover, OSC could be a better alternative of many traditional broadband light sources because of its wider spectrum and higher spatial coherence. Most OSC sources used ultrashort pulse as the pump beam since it has a high peak power. However, the ultrashort pulse pumps are usually expensive which leads to the high cost of OSC sources. In the extreme cases, an OSC source requires a large femtosecond laser system could cost hundreds of thousands of dollars. The high cost of OSC source has significantly limited its use in industry. For example, although OSC sources are almost perfect optical sources for fiber optic gyros, the high cost prevents the OSC source from being used by not only the low-precision but also the high-precision fiber optic

gyros. Based on this situation, one of objectives of this project is to design a low cost OSC source.

Other than to reduce the cost, the OSC source is designed to cover the infrared-region applications in optical communication, which uses the infrared-region roughly from 1500nm to 2000nm. Additionally, this region is also used in sensor, organic cell detecting, and spectroscopy. Till now, most of OSC only generates supercontinuum below 1750nm in wavelength. To our knowledge, there are only two ultrashort pulse pumped OSCs reported that have continuum spectra above 1750nm [25, 39]. Although the two OSCs can roughly cover the region from 1500nm to 2000nm, the high cost of these sources render them less useful in practical uses. Thus, it is a good motivation for us to design a low-cost CW pumped OSC source which can satisfy these infrared-region coverage requirements in these applications.

Chapter 2 Proposed OSC Source and Theoretical Analysis

In this chapter, a CW pumped OSC source is proposed and the principle of the OSC source will be explained. Furthermore, the theoretical analysis will be given.

2.1. Proposed OSC source

2.1.1 Introduction of design

The objective of this project is to design a low-cost OSC source whose spectrum should covers long wavelengths above 1500nm. Based on this objective, a CW pumped OSC which consists of an Er/Yb co-doped fiber (EYCDF) ring-cavity laser and a HNLF is proposed. Using CW pump for OSC generation allows OSC source to have lower cost than that of ultrashort pulse pumped OSC, since CW pumps are cheaper. Figure 2-1 illustrates the structure of proposed OSC source where an EYCDF laser is used to generate pump beam and a highly nonlinear fiber is inserted into the ring to generate various nonlinear effects that contribute to the final generation of the OSC.

The proposed OSC source adopts a ring-cavity structure which is different to the structures of other CW pumped OSC sources which were based on a single-pass structure. Figure 2-2 shows a general frame of single-pass structure. For CW pumped OSC, a major defect of sing-pass structure is that a long nonlinear fiber or very high pump power is required, since long fiber or high pump power is needed to produce

strong nonlinear effects. The high requirement of long fiber and pump power will lead a high cost of the CW pumped OSC source.

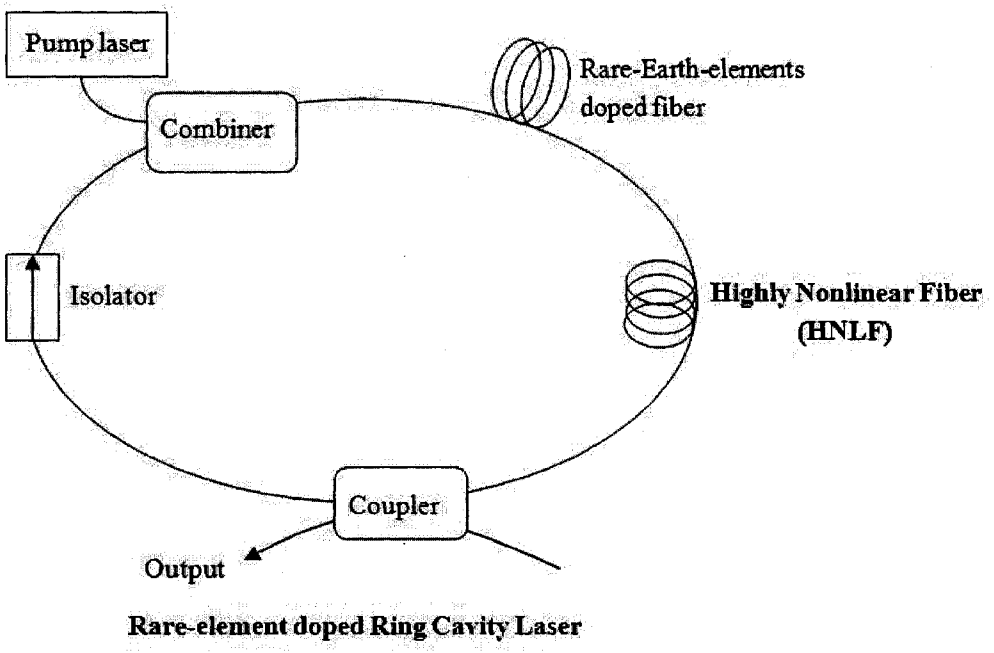

Figure 2-1 Scheme of OSC based ring cavity with HNLF

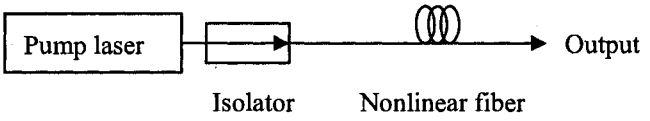

Figure 2-2 Illustration of a basic single-pass structure

Using ring-cavity structure in CW pumped OSC can effectively reduce the requirements on fiber length and pump power. Originally, the ring cavity is one of structures, which was used to generate optical pulse. Theoretical analysis and practical applications have proven that ring cavity structure can effectively reduce the requirement of pump power and the length of fiber [10]. Thus, using ring-cavity structure for OSC generation can reduce the cost of OSC source as well by avoiding

using overlong nonlinear fiber or high pump power.

Meanwhile, the CW pumped OSC source based on ring cavity structure has other features as follows:

1. Low cost:

Except of reducing cost by using relative short fiber and low pump power, ring cavity laser is helpful to save cost by using cheap devices in it. Since it is widely used and has mature technology, ring cavity laser allows common and cheap commercial devices to be used. Meanwhile, the performances of these devices are excellent and stable as well, conferring the OSC source the low cost and stable performance features.

2. Easily assembled:

In some OSC experiments, mirrors and free-space optical coupling were used. These connecting methods make these OSC sources difficult to be assembled. Unlike these OSC sources, the ring cavity structure allows the OSC source in this project to have a simple structure and all devices to be simply connected by fiber splicing.

3. Compact structure:

The ring cavity structure allows OSC to be generated with short nonlinear fiber. Thus, comparing to other CW pumped OSC, our OSC source have smaller size, which allows it to be more easily incorporated into other devices.

2.1.2 Principle of proposed OSC source

The general principle of this OSC source is simple. The ring cavity laser produces

CW seed beam. By tuning the output power of the pump laser, the power of CW seed beam can be increased. Then, the CW beam with high power is pumped into HNLF to generate OSC. By the optical coupler, the OSC beam is divided into two parts. One is the output beam of OSC source, and the other is a feedback beam which is sent back to Er/Yb co-doped fiber and is amplified. Subsequently, the amplified beam is pumped into HNLF to generate OSC beam, which will be divided into two parts again in the coupler. As a result, a stable output of OSC beam can be obtained by repeating this process.

As a major component, principles of the EYCDF ring-cavity laser need to be introduced.

Principles of Er/Yb co-doped ring cavity fiber laser

Rare-element doped fiber is the key component of a fiber laser. Ions of rare elements such as erbium, holmium, samarium, thulium, and ytterbium can absorb photons at certain frequencies and emit new photons at different frequencies. The commonly used element is Erbium (Er). Figure 2-3(a) illustrates the process of absorption and emission of photons by Er^{3+} ion. Er^{3+} ion has the highest absorption efficiency at 980nm and the highest emission efficiency at 1550nm. Thus, an Erbium doped fiber laser can convert 980nm CW beam into 1550nm beam, which is close to the ZDW of a normal HNLF. During the conversion process, most of the pump power could be lost because of the limited absorption efficiency of Er^{3+}. However the absorption efficiency can be

improved greatly by doping Ytterbium (Yb) ion and Erbium ion together into the fiber, since Yb^{3+} has much higher absorption efficiency than Er^{3+}. Yb ion cannot replace Er ion because it does not emit photons at 1550 nm with the highest efficiency. Figure 2-3(b) shows the energy-level diagram of Er^{3+} and Yb^{3+}. Yb^{3+} has an absorption efficiency at 975nm as high as 95% [40]. Thus, most of the pump photons are absorbed by Yb^{3+} and emitted by Er^{3+}. Furthermore, since the two ions have close excited energy levels, most of absorbed energy is transferred to Er^{3+} ions to emit lights at 1550nm, and this is called a cross-relaxation effect of atom energy level. By this way, higher output power can be obtained in Er/Yb co-doped fiber than that in Er doped fiber.

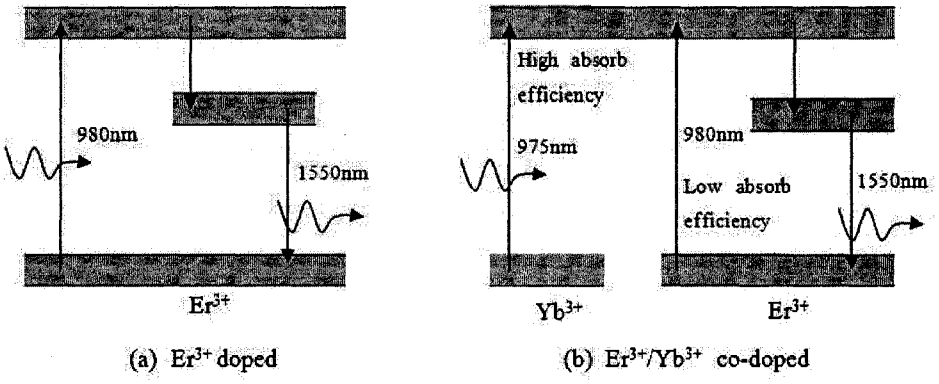

Figure 2-3 Energy-level diagrams of (a) Er^{3+} and (b) Er^{3+}/Yb^{3+} co-doped cases. In (b), Yb^{3+} ions absorb most of pump photons (source [40]).

An Er/Yb co-doped fiber (EYCDF) laser works according to the following process which is also illustrated in Figure 2-4:

(1) The beam generated by 975nm CW pump laser is sent into (EYCDF) by a WDM combiner which can couple several beams with different wavelengths into one beam to propagate in a fiber.

(2) Then, the electrons in EYCDF absorb pump photons and jump to an excited state. Initially, the spontaneous emission happens in EYCDF and produces a wide spontaneous-emission-noise spectrum which has a peak around 1550nm. The beam generated by EYCDF propagates along the ring and returns back to EYCDF.

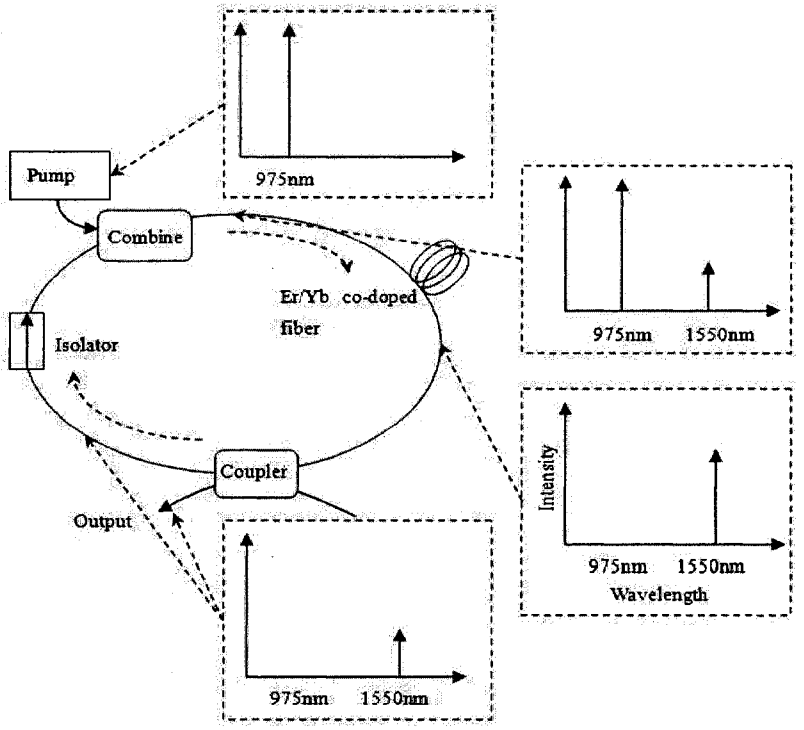

Figure 2-4 Principle scheme of Er/Yb co-doped fiber laser

(3) When the spontaneous-emission beam propagates along EYCDF, the stimulated emission happens and the spontaneous emission is suppressed. Furthermore, a certain range of frequency components around 1550nm is amplified.

(4) After being amplified in EYCDF, the stimulated-emission light is divided into two parts by a fiber coupler. One part is used as the output, and the other is used as feedback beam of laser.

(5) The feedback beam along with pump beam are coupled together by the combiner and sent into EYCDF again. Then the process will be repeated from step (3), except that a stimulated emission beam returns to EYCDF instead of a spontaneous emission beam in step (3).

Here, the isolator ensures that the laser operates at unidirectional way, since the EYCDF emits light bidirectionally along fiber at same time.

2.2. Theoretical analysis

2.2.1 Theoretical prediction

It has always been a problem in all experiments of OSC generation that the theoretical predictions are not well consistent with the result of experiments. This is because the evolution of OSC is a dynamitic process in which multiple nonlinear effects interact with each other in a very complicated pattern that is not well understood. Although the theoretical predictions are not precise, the theoretical analysis can be used to roughly describe the OSC profile by which we can know if this OSC source would satisfy the objective of this project.

Basic conditions of analysis are given firstly. In the design of this OSC source, the Er/Yb co-doped fiber produces a CW beam around 1550nm. The 1550nm wavelength is in the anomalous dispersion region of HNLF and close to the ZDW of HNLF.

For an optical pulse, the propagation process of pulse is approximately expressed by

the non-linear Schrödinger (NLS) equation. A generalized NLS equation is given as:

$$\frac{\partial A}{\partial z}+\frac{\alpha}{2}A-i\sum_{k=2}^{k_{max}}\frac{i^k}{k!}\beta_k\frac{\partial^k A}{\partial T^k}=i\gamma\left(|A|^2A+\frac{i}{\omega_0}\frac{\partial}{\partial T}\left(|A|^2A\right)-T_RA\frac{\partial|A|^2}{\partial T}\right) \tag{2.1}$$

where A is the amplitude of a pulse, $|A|^2$ represents the power of pulse, α is the loss of fiber, β_k is the k-order dispersion, T represents the physical time, γ is nonlinear coefficient, ω_0 is the center frequency of optical pulse, and T_R is the time of the nonlinear response.

Although it describes the propagation of the pulse in fiber, Equation 2.1 can also be used to describe continuous wave (CW) propagation in fiber. If we consider the CW as a pulse, the time width of CW is much longer than 5-ps. Thus, the last two items in Equation 2.1 can be neglected. Meanwhile, the higher order dispersion can be neglected when β_2 is not zero. Thus, Equation 2.1 can be simplified as:

$$i\frac{\partial A}{\partial z}=\frac{\beta_2}{2}\frac{\partial^2 A}{\partial T^2}-\frac{i\alpha}{2}A-\gamma|A|^2A \tag{2.2}$$

where A is the amplitude of CW and $A=\sqrt{P_0}\exp(i\phi_{NL})$

When CW beam propagates in a fiber, a small perturbation could be imposed in the beam. The perturbation can be cause by any reason such as noise or other nonlinear effects. Thus, the amplitude of CW beam is also expressed as

$$A=\left(\sqrt{P_0}+a\right)\exp(i\phi_{NL}) \tag{2.3}$$

where the variable a represents the small perturbation. Substituting Equation 2.3 in Equation 2.2, the solution of the perturbation a is given as [10]:

$$a(z,T) = a_1 \exp[i(Kz - \Omega T)] + a_2 \exp[-i(Kz - \Omega T)] \quad (2.4)$$

where K is wave number, Ω is the frequency difference between the perturbation and CW.

It can be found in Equation 2.4 the perturbation produces two components at frequencies $\omega_0 \pm \Omega$ (ω_0 is the frequency of CW).

In fact, the above deductions can represent the generation of MI effect that induced two side lobes in spectrum. Figure 2-5 illustrates the autocorrelation trace and spectrum of MI effect of a continuous wave [41]. The frequency of the CW is at 1550nm. In the left part of Figure 2-5, the upper picture shows the CW signal in time domain and the bottom picture shows the spectrum of the CW signal. When it experiences anomalous dispersion, the CW is transformed to a train of pulses (upper right part in Figure 2-5). Meanwhile, two side lobes appear at both sides of CW spectral peak (bottom right part in Fig 2-5). Then, the spectrum will be broadened toward red and blue directions. The broadening process is schematically shown in Figure 2-6. Here, it is assumed that the nonlinear fiber has normal dispersion below 1550nm and anomalous dispersion above 1550nm.

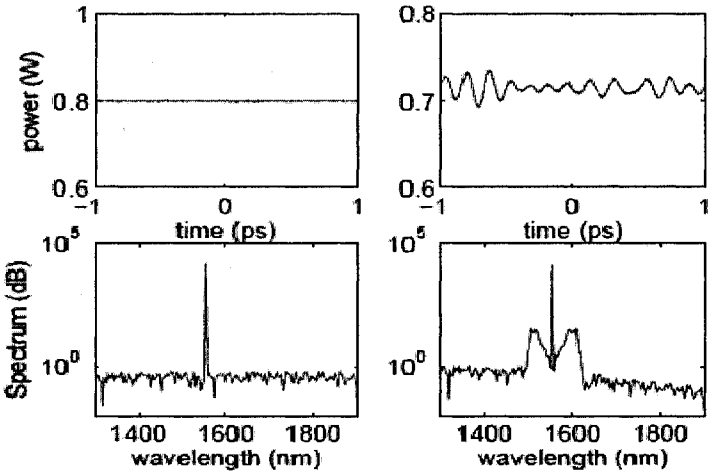

Figure 2-5 Autocorrelation trace and spectrum of CW showing evidence of MI effect. (source [41]).

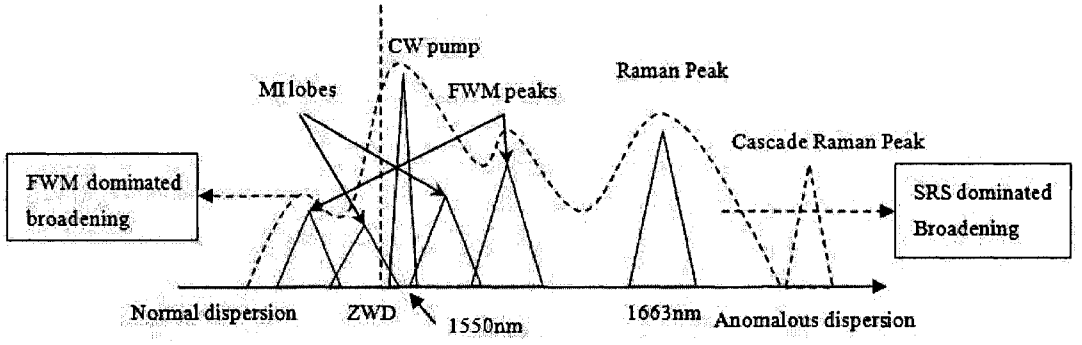

Figure 2-6 Scheme of spectrum broadening

When pulses are formed, the beam propagation is governed by Equation 2.1 instead of Equation 2.2. In Equation 2.1, the right part represents nonlinear effects such as SPM, SRS and FWM.

In this experiment, a long HNLF is used. Thus, the effective length L_{eff} in Equation 1.3 is large. The large value of L_{eff} and low dispersion around ZDW will induce SPM occurring at the pump peak and MI lobes. Furthermore, SPM allows the phase matching condition of FWM to be fulfilled. Thus, FWM effect will generate Stokes and anti-Stokes peaks at normal and anomalous dispersion regions and broaden the

spectrum toward red and blue directions (Figure 2-6).

In Figure 2-6 we can see that, subsequently, in anomalous dispersion region, SRS dominates the spectrum broadening toward long wavelength. High dispersion values at these wavelengths far away from ZDW make the phase-matching condition of FWM hard to be fulfilled. Thus, FWM effect is hard to occur at further wavelengths away from pump peak. The frequency shift of FWM peaks depends on specific dispersion distribution. In contrast, SRS effect is determined by the fiber length and the pump power instead of phase matching condition. Therefore, the high peak power values of the pulses and long fiber will induce intense SRS effect. The first order Raman Stokes peak of CW pump is around 1663nm which is exactly 13THz, a characteristic value for frequency shift of Stokes peak, away from pump peak. Considering that the peak power of generated pulses is very high after they have experienced SPM induced pulse compression, it is possible that cascaded Raman Stokes peaks are generated. Thus, like other CW pumped OSC, the spectrum broadening in anomalous region is dominated by SRS effect.

In normal dispersion region, the spectral broadening is dominated by the FWM effect. However, it is difficult for the FWM effect to broaden spectrum in a great range because of the high dispersion values. Additionally, the SRS effect can transfer the power from short-wavelength region to long-wavelength region. As a result, the FWM effect at short-wavelength region is suppressed. Therefore, the spectral broadening toward short wavelength is relatively weak.

In Figure 2-6, the dash curve is actually a rough prediction of the shape of the OSC spectrum. To summarize, the spectrum evolution should be dominated by MI and SRS, since the wavelength of pump beam is chosen at anomalous-dispersion region of HNLF and CW pump is used in this OSC. More specifically, at the spectrum evolution at long wavelengths is dominated by SRS effect, whereas the spectrum broadening at short wavelengths is dominated by MI effect. Additionally, the FWM effect also contributes to the spectrum broadening at short wavelengths.

2.2.2 Experimental parameters

In this work, to control the generation of nonlinear effects, we can modify two parameters which are the power level of the pump and the length of nonlinear fiber.

In these nonlinear effects, SRS only occurs either at quite high pump power or when long fiber with low loss is used. Comparing to SRS, other nonlinear effects such as SPM, FWM and MI can occur at lower pump power or using a shorter fiber. Additionally, according to theoretical prediction, SRS effect is essential in OSC generation, since it dominates the spectrum broadening in long-wavelength region. Thus, we estimate the experimental parameters, pump level, and fiber length based on the conditions under which SRS effect can take place.

Firstly, a proper length of nonlinear fiber should be decided. Here, the length of the nonlinear fiber can be roughly estimated by referring the fiber length of a CW pumped OSC conducted by Akheelesh K. Abeeluck, et al., [34]. The OSC was obtained when

pump power is 7W with 1.5km nonlinear fiber. Considering the ring cavity structure can reduce the requirement on the length of nonlinear fiber, it is inferred that the OSC could be generated with a nonlinear fiber whose length is shorter than 1.5km. Thus, the fiber length is estimated to be about 1km (L=1km). In this experiment, we chose the HNLF made by Sumitomo Electric Inc. The nonlinear coefficient γ of the HNLF is 17 $(\mathrm{km}\cdot\mathrm{W})^{-1}$, Raman gain coefficient g_R is 6.0 $(\mathrm{km}\cdot\mathrm{W})^{-1}$, and attenuation α is 0.14 (0.6dB/km)

Next, the pump power will be estimated. Firstly, it can be known that the effective length of fiber is 0.93km by using Equation 1.3. Then, according to Equation 1.5, the threshold power is about 2.8W. In other words, the incident optical power of the HNLF has to be at least 2.8W. Considering the incident beam is converted from the pump beam by the Er/Yb doped fiber, the pump power should be at least 7W if the power conversion efficiency of Er/Yb fiber was 40% as we assumed. The combination of 7W pump power and 1km HNLF of an OSC source is acceptable for practical use.

Chapter 3 Experimental Analysis and Results

In this chapter, experimental setup will be given and results will be analyzed. Based on the analysis, the main mechanism of OSC evolution will be discussed. Finally, the performance of this OSC will be compared to other CW pumped OSC.

3.1 Experimental setup

This final experimental setup is shown in Figure 3-1.

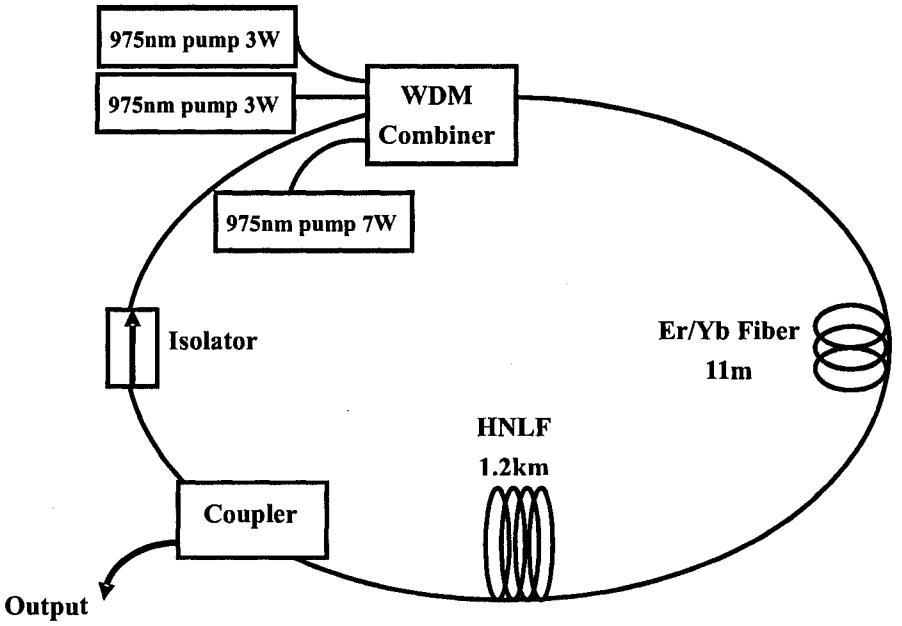

Figure 3-1 Schematic view of the experiment set-up of OSC source in our experiment.

Experimental devices

A list of experimental devices used in this work is shown in Table 2.

Table 2 List of experimental devices

Devices	Number	Manufacturer	Model/Part Number
Experimental devices			
Pump laser(3W)	2	EM4, Inc	EM337
Pump laser(7W)	1	EM4, Inc	EM327
WDM combiner	1	OFS, Inc	TFB1310
Er/Yb co-doped fiber	1 (11m)	OFS, Inc	ErYb130
Highly nonlinear fiber	1 (1.2km)	Sumitomo Electric Industries, Ltd	HNL-DSF

1) Pumps:

Three 975-nm multi-mode un-cooled semiconductor CW lasers are used as the pump lasers whose maximum output power are 3W, 3W and 7W, respectively. As estimated in Section 2.2.2, the total pump power should be above 7W. Thus, three pump lasers whose total optical power is 13W provide enough pump power for OSC generation. The 3dB bandwidth of output spectra of all three pump lasers are 3nm. Multi-mode semiconductor laser are cheaper than narrow line-width laser because there is a lower requirement on the number of modes.

2) WDM combiner:

As shown in Figure 3-1, a WDM combiner is used to combine three pump lasers and a feedback beam together and launch the combined beam into the Erbium/Ytterbium co-doped fiber.

The WDM combiner is a taped fiber bundles with six Er/Yb doped multi-mode input fibers, one Er/Yb doped single-mode input fiber and one un-doped output fiber. The center wavelength of the combiner is 1550nm, and the handling input power is 35 W.

Three pump lasers are spliced with three of the six multi-mode input fibers of the WDM combiner. Single-mode input fiber is used to receive the feedback beam. The combined beam is sent out from the un-doped output fiber to the Er/Yb co-doped fiber.

3) Er/Yb co-doped fiber:

As mentioned in Section 2.1.2, Er/Yb co-doped fiber (EYCDF) can convert 975nm pump beam to a 1550nm beam. The EYCDF in this OSC has a core diameter of 6.6 μm, a 130 μm star-cladding-shaped inner cladding with a numerical aperture of 0.45, and a polymer outer cladding. The double claddings structure can confine the pump beam in the core zone in order to let the Er^{3+} and Yb^{3+} in the core absorb as many pump photons as possible. The absorption efficiencies at two absorption peaks, 975nm and 1535nm, are 800dB/m and 29dB/m respectively. The major absorption efficiency at 975nm is relatively high.

The EYCDF absorbs pump photons at 975nm and emits a seed beam at 1568nm using this experiment setup. Then the seed light is pumped into a 1.2 km HNLF. The length of HNLF is close to the estimated length mentioned in Section 2.2.2, 1km.

4) Highly nonlinear fiber:

Zero-dispersion wavelength (ZDW) of the 1.2km HNLF is at 1560 nm which is close to the wavelength of the seed light produced by EYCDF (1568 nm). The dispersion slope at 1560nm is $0.03\ ps/nm^2 \cdot km$ and the nonlinear coefficient of the HNLF is $17\ W^{-1} \cdot km^{-1}$. The loss of the HNLF is $0.6 dB/km$. An OSC formed in this HNL will be transmitted to a fiber coupler.

5) Fiber coupler:

The fiber coupler will split the OSC beam into two beams. One is the output and the other is a feedback beam of ring cavity laser. The splitting ratio (feedback to output) of the fiber coupler is 70/30%. Since the wavelength region around 1550nm has numerous applications, these fiber couplers usually have a "window" from 1510nm~1590nm. A "window" is referring to as the wavelength range within which the insertion loss is very low. Figure 3-2 shows a typical insertion loss spectrum of a 50/50% fiber coupler. From this figure, we can find the insertion loss increases rapidly in the long wavelength region (above 1700nm). The high loss at long wavelengths will limit the spectrum broadening of OSC toward the red. Therefore, most fiber couplers are band limited devices.

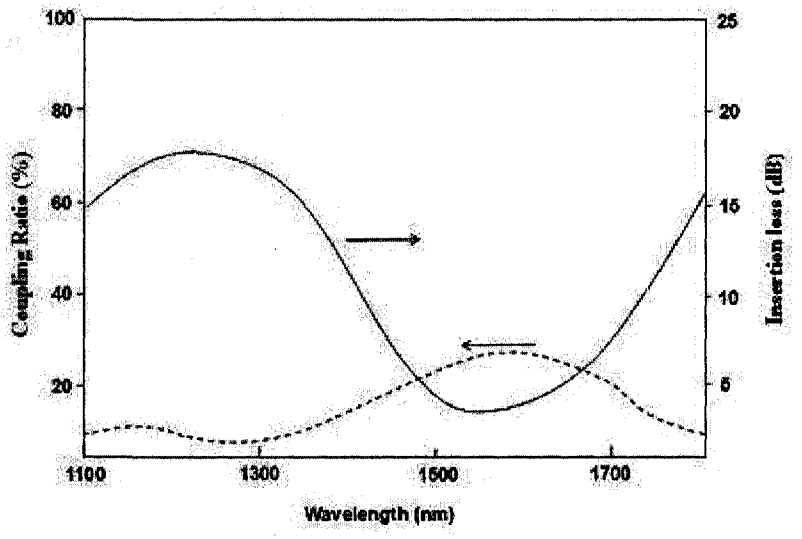

Figure 3-2 Typical insertion loss spectrum of a 50/50% coupler where the window is from 1500nm to 1650nm (source www.trioptics.com/products/coupler.php)

Downstream of the fiber coupler, the feedback beam will be launched into an optical

isolator.

6) Optical isolator

An optical isolator is like a filter in which only light with selected propagating direction is allowed to pass in the cavity. The handling backward power of the isolator is 2W. Finally, the ring cavity is constructed after the isolator is spliced with the SM input fiber of the taped fiber bundles.

Measurement instruments and experimental tool

Table 3 Measurement instruments and experimental tool in this experiment

Measurement Instrument			
Optical Power Meter	1	ILX Lightwave	OMM-6810B (with OMH6727B InGaAs dectecting head)
Optical Spectrum Analyzer	1	ANDO Electric Co.,Ltd.	AQ6317B
Monochromator	1	CVI	Instruments Digikrom 240
Photovoltaic InSb detector	1	Optikon	I-345-IS
Experimental Tool			
Fiber splicer	1	Ericsson	FSU-995

In this work, we have used three measurement devices (Table 3), an optical power meter, an optical spectrum analyzer (OSA), and a Monochromator together with a photovoltaic Indium-Antimony (InSb) detector.

1) Optical power meter:

The power meter is used to measure the optical power of OSC source. The Indium-Gallium-Arsenic (InGaAs) detecting head of the power meter has a measurable range from 950nm~1650nm, and the measurable power of detecting head is from

30dBm (1W) ~ -40dBm (10^{-4}mW). The damaging threshold power of the power meter is 40dBm (10W).

2) Optical spectrum analyzer (OSA):

The OSA is used to analyze the spectral range lower than 1750nm. It has a measurable range from 650nm~1750nm. The maximum input optical power of the OSA is 100mw (20dBm) which is the total power of every frequency component in measurable spectrum.

3) Monochromator:

Since the upper limit wavelength of the OSA is 1750nm, a monochromator with an Indium-Antimony (InSb) semiconductor photovoltaic detector is used to measure the long wavelength spectrum of greater than 1750nm. A monochromator is an optical device that selects a narrow band of light from a wider range of wavelengths and transmits the selected narrow-band light to the input of detector. In this work, a long-wavelength band (above 1700nm) is selected by the Monochromator. Then, the selected narrow-band beam is launched into the InSb photovoltaic detector which has a highly sensitive measurable range from 1μm to 5.5μm.

3.2 Experiment methods

3.2.1 Loss in EYCDF ring cavity laser

Since the OSC source in this experiment is based on a ring cavity laser, the quality of

the ring cavity laser is crucial to the resulting OSC. Loss in the ring cavity laser is the major limit of OSC generation. High loss in ring cavity will cause the optical power pumped into HNLF to be too low to generate various nonlinear effects. The loss in ring cavity mainly consists of the loss of the devices and the splicing. Since the loss in devices is not likely to be avoided, controlling the splicing loss becomes essential for controlling total loss.

Splicing loss is due to different mode-field diameters (MFD) of two optical fibers. When a beam passes through the interface between two fibers, the beam cannot be completely coupled from one fiber to another because of the unmatched MFDs. Simply splicing fibers together without considering the MFD matching cannot ensure low splicing loss.

To obtain a high quality splicing, the key is to match the MDF of two fibers. A fusion splicer matches the MDFs by fusing two fibers together in order to make the transition of the beam from one core to another as smooth as possible. During this process, the fusion time is a key parameter. The operation mode of the fusion splicer, auto mode-field matching, usually can control fusion time very well in most cases. For those cases that the automatic mode does not work well, a simple method, as shown Figure 3-3 where the Fiber 1 and 2 are two fibers to be spliced together, can be used to control the fusion time. In Figure 3-3, the 1550nm light source launches a beam with certain power, into fiber 1. An optical power meter is placed at the output end of fiber 2 to measure how much optical power is transferred from fiber 1 to fiber 2. During the

splicing process, the output power of fiber 2 can be observed on optical power meter.

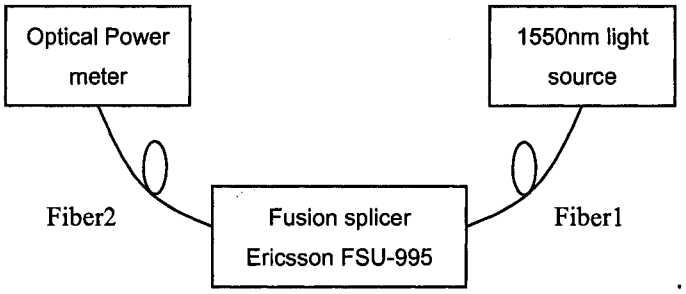

Figure 3-3 Experiment setup for splicing undoped fibers

More specifically, first, the parameters, such as fiber type and MFD, are set in fusion splicer. When the two fibers are placed in the fusion splicer and the splicing process starts, the output power on the optical power meter starts to increase. As soon as the output power reaches the maximum value, the splicing process is manually terminated by shutting off the arc in fusion splicer. Using this method the splicing loss of two un-doped fibers can be maintained lower than 0.1 dB.

3.2.2 Power conversion efficiency of Er/Yb co-doped fiber

For a rare-element doped fiber, the efficiency of converting pump power to output power is referred to as the power conversion efficiency (PCE). PCE is an important conversion index of the performance of a fiber laser. For OSC generation in this work, PCE has critical impacts on the performance of OSC source because the OSC generation depends on how high the incident power is pumped into the nonlinear medium. Low PCE will lead to the requirement of higher pump power. Obviously, high pump power is disadvantageous to be used in a practical OSC source.

The PCE is determined by several factors such as the concentration of the rare elements, the length of the doped fiber, the pump power, and the splicing loss between EYCDF and the pump laser. High rare-element concentration and long EYCDF can increase the number of free electrons and holes. However, overlengthed EYCDF reduces PCE, because a number of generated photons will be absorbed by EYCDF again. High pump power and low connecting loss will allow more pump power to be absorbed by ions in EYCDF. Since the concentration of a doped fiber cannot be changed after it is made, only the fiber length, pump power and loss can be modified. In this experiment, an 11m EYCDF is used, and PCE was measured at different power levels.

Since the EYCDF emits lights at both forward and backward directions along the fiber, the PCE is the ratio of the total power of both direction lights to the pump power. Test data are listed in Table 4 and the test method is illustrated in Figure 3-4 where the forward and backward power values are measured individually.

Table 4 Data of power conversion efficiency of EYCDF

Forward (mW)	Backward (mW)	Power summation (For+Back) (mW)	Pump power (mW)	Efficiency
0.01	0.14	0.16	90	0.2%
7.8	19.9	27.7	220	12.5%
33.0	72.7	105.7	430	24.6%
67.3	128.5	195.8	650	30.1%
108.1	191.2	299.3	850	35.2%
151.3	253.7	405.0	1070	37.9%
201.5	317.6	519.1	1280	40.6%
257.0	385.5	642.5	1500	42.8%
312.6	452.5	765.1	1700	45.0%

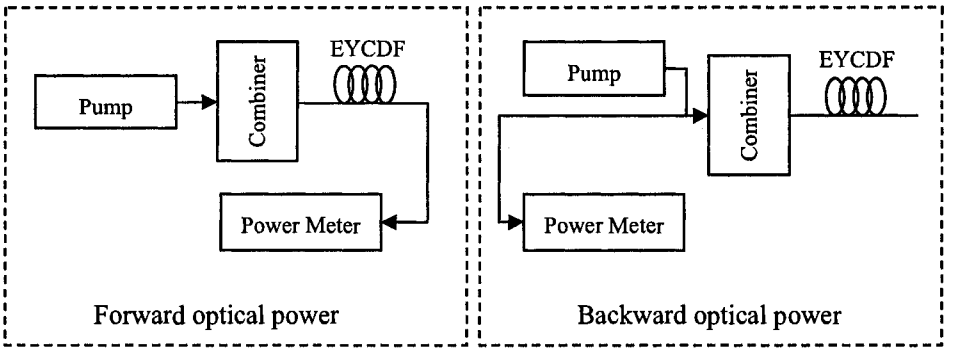

Figure 3-4 Schematics of measuring power conversion efficiency of EYCDF

In this test, the PCE at higher pump power of more than 1.7W is not measured in order to avoid damaging the measurement instrument by the high optical power. From the data in Table 4, the PCE keeps increasing when pump power rises, and it reaches the maximum value 45% at pump power 1.7W. The 45% PCE is higher than our expectation 40%. Therefore, it is inferred that the PCE could be higher when pump power is increased further.

3.3 Experimental results

3.3.1 Evolution of OSC

The spectral evolution as a function of the pump power is shown in Figure 3-5.

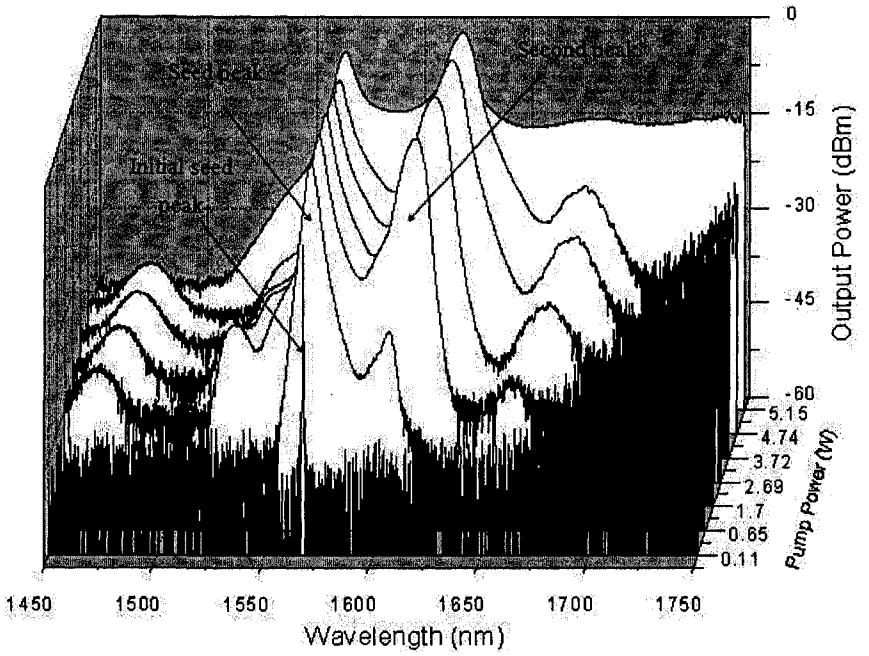

Figure 3-5 Evolution of OSC as the function of pump power

As shown in Figure 3-5, the ring cavity initially produces a seed beam at 1568nm (also see Figure 3-8) when the pump power is 0.11W. Subsequently, the seed-beam peak keeps being broadened by SPM effect with increasing pump power. Just as we mentioned previously, the SPM-induced spectrum broadening is due to the fact that intense fluctuations of CW beam are converted into the phase fluctuations by SPM, and the instantaneous phase fluctuations generate new frequencies around the center frequency. Then, SPM induced spectrum broadening is further enhanced while the CW light propagates down the fiber and the pump power is being increased.

When the pump power approaches 0.65 W, the second peak appears at 1608 nm. This peak is not generated due to any nonlinear effects. This can be proved by an experiment in which two spectra are recorded respectively: one uses an 11km dispersion shift fiber

instead of HNLF, and the other does not use any fiber. Figure 3-6 is the output spectra of the Er/Yb-fiber ring cavity with and without an 11 km DSF. A peak around 1608 nm is seen in the both cases, suggesting that the peak at 1608nm is not caused by any nonlinear effect. The reason for the appearance of this peak is thought to be the saturation of the number of the excited electrons which can emit 1568nm light, thereby allowing the absorption of the optical power by other electrons which jump onto another excited state to produce the 1608nm light.

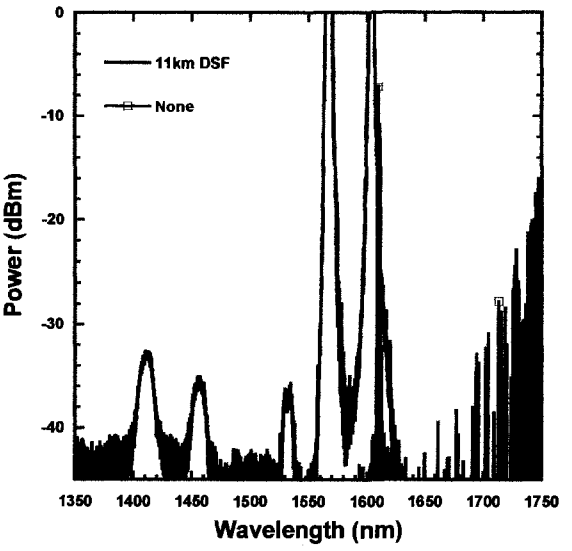

Figure 3-6 Output spectra of the Er/Yb-fiber ring cavity when the HNLF is replaced by 11 km DSF and removed.

From Figure 3-5, we also can find the peak at 1568nm (seed peak) does not grow after the 1608nm peak is generated, whereas the 1608nm peak (second peak) keeps growing with the increase of pump power. This is another proof of the saturation of the number of the excited electrons emitting 1568nm light and the excitation of other electrons emitting 1608nm light.

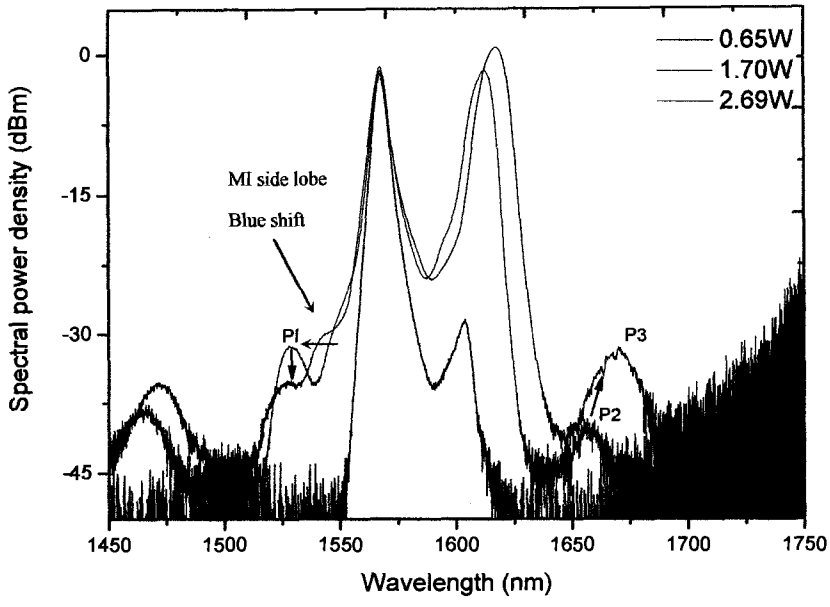

Figure 3-7 FWM and MI effects in different level of pump power, where P1, P2, P3 are the FWM anti-Stokes and Stoke lines.

MI effect of seed beam can be observed in Figure 3-7 where the left side lobe shows blue shift in frequency, which is a typical characteristic of MI effect. The emergence of MI effect shows that CW is broken up into pulses. The existence of MI effect can be proved by the blue shift in the frequency of the left side lobe (See Figure 3-7 and 3-9)

When the pump power is 1.70W, the anti-Stokes and Stokes peaks produced by the FWM is observed at 1528nm and 1657nm, respectively. At these positions, phase-matching condition of FWM is fulfilled because of SPM effect. In Figure 3-7, the FWM effect appears at two of the three pump power levels. When the pump power is increased from 1.70W to 2.69W, the power of anti-Stokes peak P1 decreases and the power of Stokes peak P2 increases. This is due to the Raman effect which transfers the power from the short-wavelength region to the long-wavelength region.

In Figure 3-7, the peak P3 actually consists of two peaks, the FWM Stokes peak and SRS Stokes peak. A detailed view is shown in Figure 3-8. The wavelengths of these peaks in Figure 3-8 are shown in Table 5.

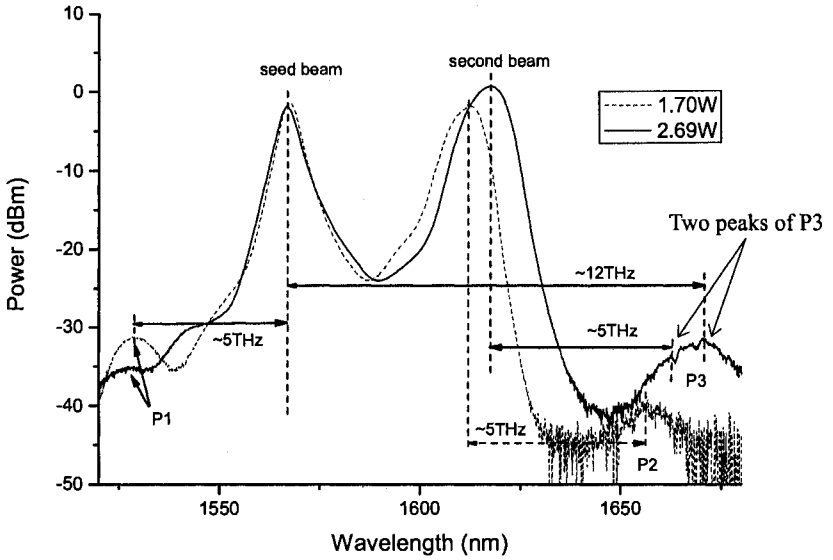

Figure 3-8 Details of the spectrum when pump power are 1.70W and 2.69W.

Table 5 Wavelengths of main peaks when pump power are 1.70W and 2.69W

Peak Name	Wavelength	Frequency	Pump Power
P1	1528nm	196THz	1.70W/2.69W
Seed beam	1568nm	191THz	1.70W/2.69W
Second beam	1612nm	186THz	1.70W
Second beam	1618nm	185THz	2.69W
P2	1657nm	181THz	1.70W
The minor peak in P3 (FWM peak)	1663nm	180THz	2.69W
The major peak in P3 (SRS peak)	1673nm	179THz	2.69W

In Figure 3-8, the peaks, P1, P2, and the minor peak in P3 are the Stokes peaks and anti-Stokes peaks of FWM. The major peak in P3 is the SRS Stokes peak. The Stokes peak of FWM exhibits a little frequency shift, since the wavelength of the second peak shifts from 1612nm to 1618nm, when pump power is increased from 1.70W to 2.69W.

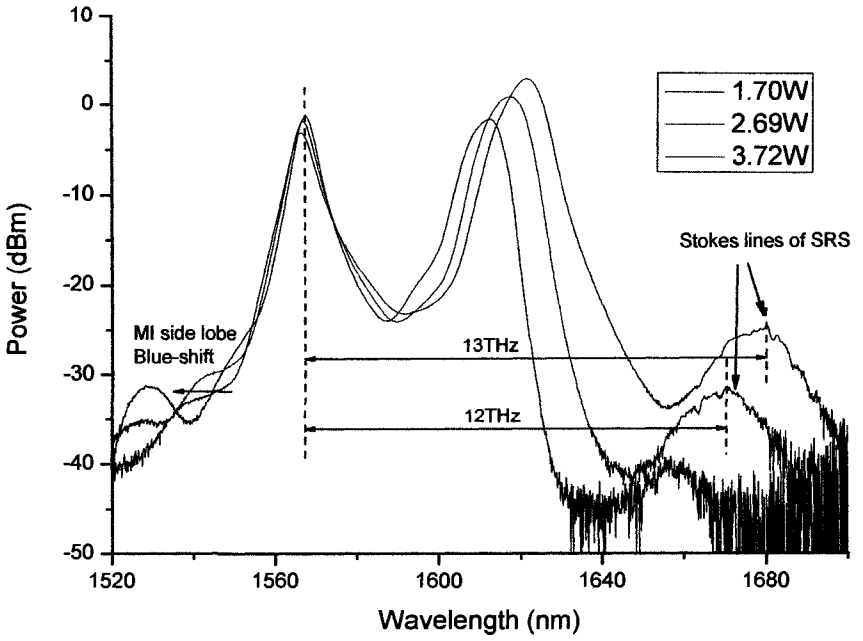

Figure 3-9 SRS peaks when pump power are 2.69W and 3.72W

Figure 3-9 shows the growing of the Stokes peak of SRS. When pump power is 2.69W, the frequency difference between of them is about 12THz. When pump exceeds 3.72W, the frequency difference between of them approaches 13THz and remains unchanged afterwards. As we mentioned in Section 2.4, 13THz is the typical value of frequency difference between pump power and Stokes peak of SRS.

When the pump power is above 3.72W, the structure of the spectrum does not change much, except that the seed peak and the second peak are being broadened by SPM with increases in the pump power. Finally, the OSC spectrum forms, resulting from a combination of the nonlinear effects SPM, FWM and SRS, when the pump power has arrived at 5.15 W.

3.3.2 Output power

Table 6 and Figure 3-10 show the output power of the OSC source as a function of the pump power. The output power data are measured by an optical power meter. Models and parameters of optical power meter are shown in Table.3.

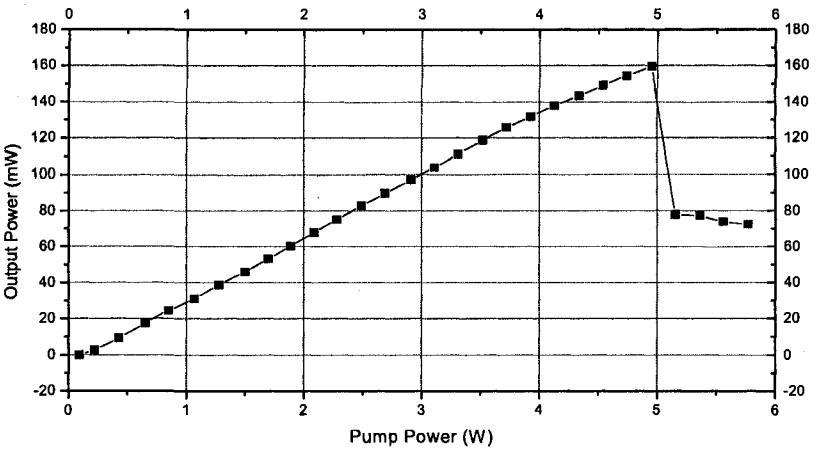

Figure 3-10 Output optical power of the OSC source as a function of 975 nm pumps power

Table 6 Output power of this OSC source.

Pump Power (W)	OSC Power (mW)	Pump Power (W)	OSC Power (mW)	Pump Power (W)	OSC Power (mW)
0.09	0	1.89	60.3	3.93	131.8
0.11	0.001	2.09	67.9	4.13	138
0.22	2.9	2.28	75.3	4.34	143.4
0.43	9.3	2.49	82.9	4.54	149.2
0.65	17.5	2.69	89.8	4.74	154.6
0.85	24.6	2.91	97.1	4.95	159.6
1.07	31.2	3.11	103.9	5.15	77.9
1.28	38.7	3.31	111.5	5.36	77.5
1.50	46.2	3.52	118.8	5.56	74.1
1.70	53.3	3.72	125.8	5.77	72.6

In Figure 3-10, the output power reduces suddenly at the pump power of 5.15W, when the OSC spectrum has formed. The power decrease is most likely caused by the

limit on measurable range of the power meter. The InGaAs detecting head of the power meter has a measurement range from 950nm to 1650nm. In other words, the power data measured with power meter only reflects the power change in the range from 950nm to 1650nm. Furthermore, when the OSC spectrum forms, much power is transferred to the spectrum above 1650nm which exceeds of the measurable range of the power meter. Therefore, the measured power value is not the actual total output power, which should be much greater than the measured value. Unfortunately, we can find proper instrument to measure the total output power.

The deduction that the power is transferred to the spectrum above 1650nm can be proved by observing and comparing the spectra before and after OSC has formed using an OSA. The spectra, before and after OSC formed, are shown in Figure 3-11, where the range of wavelength is from 950nm to 1750nm. We can find that the spectral power density at most parts of the region, from 950nm to 1650nm, decreases after OSC has formed. Especially, the second peak which has high power decreases by 9.3 dB, from 3.3dBm to -6dBm. The power decrease in these parts is consistent with the result measured by the power meter. Furthermore, we can find that the spectral power density from 1650nm to 1750nm is much higher after OSC has formed than that before. The observed result proves that the output power does not really decrease but because it exceeds the measurable wavelength range of the power meter.

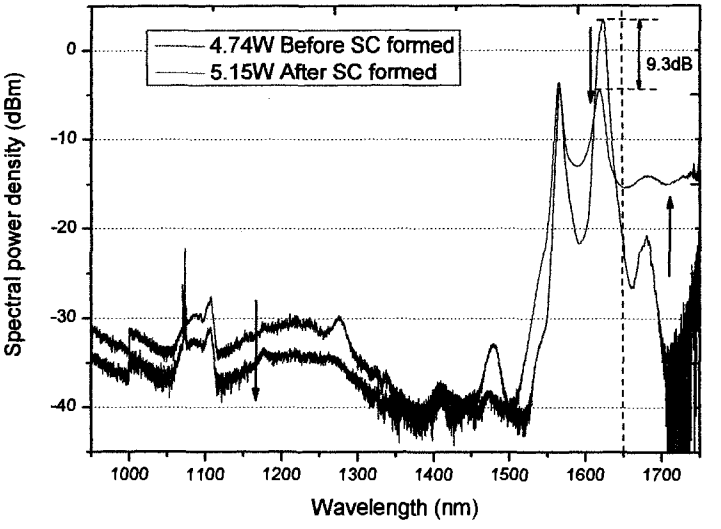

Figure 3-11 Spectra before and after OSC formed, from 950nm to 1750nm

Considering that part of pump power is transferred to the part of the spectrum at long wavelength, the OSC spectrum is believed to have another part in the region greater than 1750nm which cannot be observed either with the OSA or the power meter.

3.3.3 Spectral coverage of this OSC source

In the previous section, it is inferred that there is a part in OSC spectrum above 1750nm that cannot be observed because of the limits of the measuring devices. Therefore, a monochromator with a Photovoltaic InSb detector is used to observe the long wavelength spectrum. The Photovoltaic InSb detector is highly sensitive between wavelengths of 1μm and 5.5μm. However the handling power of the detector is as low as 200μW. To measure the OSC source that has a high optical power, an attenuation mirror has to be used upstream of the monochromator.

Figure 3-12 and Figure 3-13 show the spectrum below 1750nm and above 1700nm.

The result in Figure 3-12 is recorded by an OSA with resolution 0.5nm. The result in Figure 3-13 is recorded by the monochromator where the measurement resolution is 2nm and a 25dB attenuation mirror is used. In Figure 3-13, the discontinuity in shape of the spectrum between 1850nm to 1900nm is caused by noise. Since a high attenuation is used, the reduced optical power causes that part of spectrum to be quite easily interfered by noise.

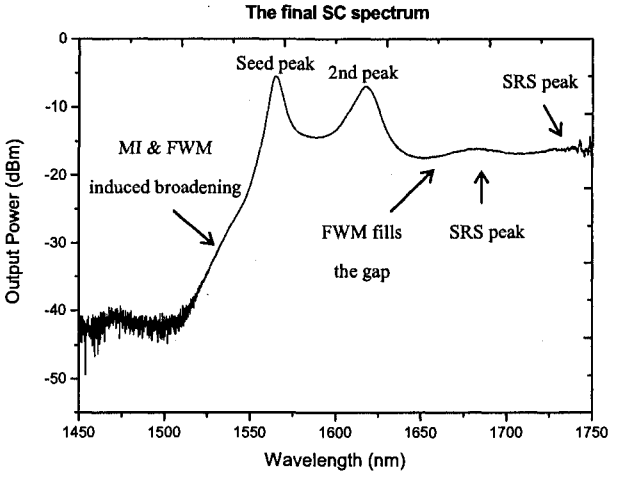

Figure 3-12 OSC spectrum below 1750nm

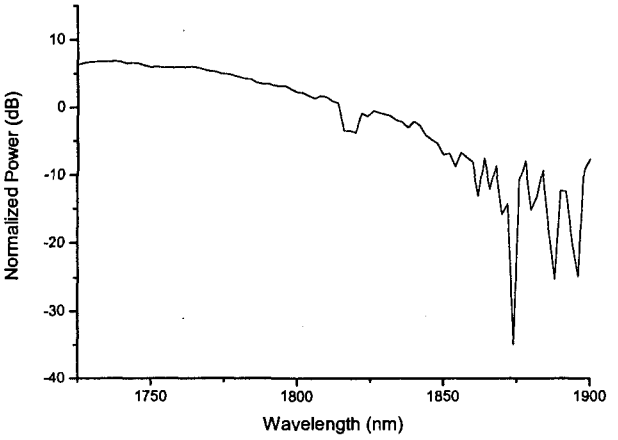

Figure 3-13 OSC spectrum above 1700nm

According to the result, the 15dB bandwidth of the OSC spectrum above 1750nm is about 150nm in wavelength, and adding the bandwidth 200nm of the spectrum below 1750nm to the 150nm, the total bandwidth of the OSC is 350nm, from 1550nm to 1900nm in wavelength.

3.3.4 Reliability of experimental result

Figure 3-14 shows the output spectra measured seven times at roughly same pump power level which is 5.2W. The spectrum coverage and spectral power densities are little different between them because the values of pump power cannot be tuned to an exactly same values at every time. In addition, change of the room temperature all contributes the change of output result. The impact of room temperature to the result is minor than that of pump power.

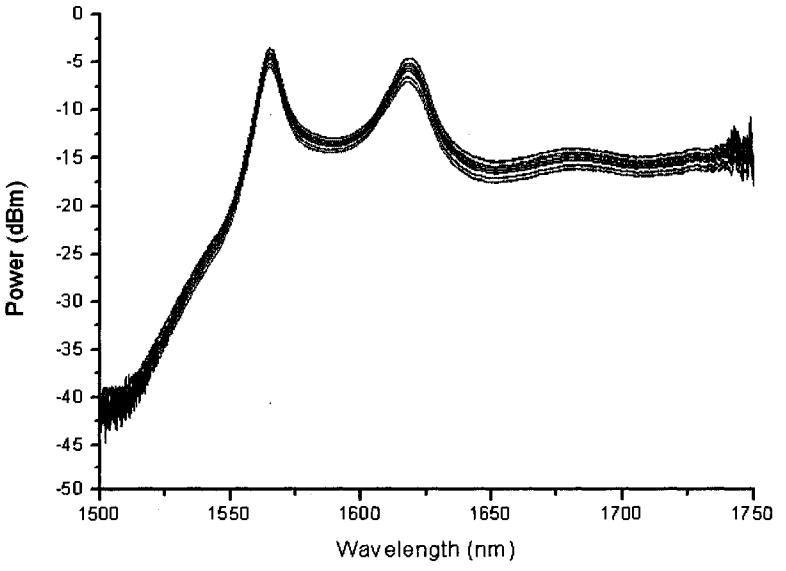

Figure 3-14 Output spectra measured seven times

To show the repeatability of our experiment, the lower-limit wavelengths and average spectral power densities of the seven spectra are given in Table 7. Since, the upper-limit wavelength cannot be decided due to the intense noise of monochromator which causes intense interference around upper-limit wavelength of the spectrum, only lower-limit wavelengths of 25dBm bandwidths of the seven results are given.

Table 7 25dBm lower-limit wavelengths and average power densities

Number	lower-limit wavelength (nm) (25dBm bandwidth)	Average power density (dBm)
1	1539	-16.5
2	1544	-18.5
3	1542	-17.6
4	1541	-17.1
5	1540	-16.9
6	1543	-18.0
7	1541	-17.3

According the data in Table 7, the average lower-limit wavelength (25dBm) of our OSC source is 1541.43nm with a margin of error of $\pm 1.27nm$, based on the seven measurement results when the confidential level is 95%. The mean of average power density is -17.4dBm with a margin of error of $\pm 0.5dBm$, when the confidential level is 95%.

Chapter 4 Discussions, Conclusions and Future Works

4.1 Discussions

4.1.1 Evolution mechanism and comparison with theoretical prediction

In theoretical prediction, four nonlinear effects, MI, SPM, FWM and SRS are expected to contribute to OSC formation. Meanwhile, we expect that the evolution would be dominated by MI and SRS effects.

From the experiment result, the four nonlinear effects were observed in the generation of OSC as we expected. However, the real evolution mechanism is different from the theoretical prediction. The mechanism is SPM and SRS effects dominated evolution instead of MI and SRS dominated.

Firstly, in the evolution, the SRS Stokes peaks mainly contribute to broadening the coverage of the spectrum. The seed peak and the second peak generate SRS effect. The SRS peak generated by seed beam extends spectrum to 1680nm (the left SRS peak in Figure 3-12). The appearance of the second peak is unexpected in theoretical predictions because it is not caused by any nonlinear effect. The unexpected second peak with high power generates a SRS peak and broadens spectrum to 1750nm (the right SRS peak in Figure 3-12). The reasons and mechanisms of the spectrum broadening above 1750nm are not well understood. However, it is thought that the

spectrum broadening above 1750 may be contributed by cascaded SRS Stokes peaks generated by the second peak. From Figure 3-11, we can find that the power of the second peak decreases very much after the OSC formed. Thus, it is deduced that the power for broadening the spectrum is mainly provided by the second peak. By calculation, we can find that the second peak generates a first-order Stokes peak around 1744nm which also can be observed in Figure 3-12. If the first-order Stokes peak could generate SRS effect, the second-order Stokes peak should be at 1888nm which roughly is the upper-limit wavelength of this OSC. Therefore, it is possible that the spectrum broadening above 1750nm is achieved by cascaded Raman Stokes peaks. Nevertheless, these deductions require further investigations and analysis.

Secondly, SPM effect contributes to spectral peaks broadening throughout entire evolution. Meanwhile, the strong SPM induces FWM and MI to occur. SPM in seed peak and the second peak make the phase matching condition of FWM to be fulfilled. Therefore, the seed beam and the second beam produce FWM effect and seed two Stokes peaks in normal and anomalous dispersion region. The anti-Stokes peak is the seed of broadening spectrum to short-wavelength region, and the Stoke peak of FWM fills the gap between the second peak and Raman peak generated by the seed peak and helps to form a flat spectrum. Strong SPM effect also induces MI effect to occur in seed peak. Like FWM effect, MI effect generates two side lobes at normal and anomalous dispersion region. The phenomenon, SPM inducing MI effect, can be explained as that SPM induces the spectral peak of the seed beam to be broadened into the gain spectrum

of MI effect. The frequency components in gain spectrum can be seen as small perturbations, which lead to the formation of two side lobes of MI effect. Additionally, the MI effect induces the break-up of CW to pulses. Considering these pulses propagate in anomalous dispersion region, it is inferred that these pulses are compressed as the result of interaction of SPM induced positive chirp and anomalous dispersion. The high peak power of the compressed pulses is favorable to the generation of intrapulse Raman scattering, which also contributes to spectral broadening.

Generally, SPM and SRS effects dominate the evolution of OSC in this work. The evolution pattern is new in CW pumped OSCs. In most CW pumped OSCs, MI and SRS are considered as the major nonlinear effects which contribute to form OSC. In this work, this new evolution mechanism is induced due to the ring-cavity structure is used in this OSC source. As mention in Section 2.1.1, the ring-cavity structure can increase the effective length of nonlinear fiber which induces intense SPM and SRS effect. Furthermore, strong SRS effect suppresses MI effect.

It should be noted that we theoretically predict the existence of a small spectrum broadening at short-wavelength region. However, in the practical experiment, we find that the broadening at short-wavelength region is almost eliminated by strong SRS. This is because the ring cavity structure gives rise to a long effective length of fiber which enhances the SRS. Furthermore, the strong SRS prevents power to be transferred from pump beam to anti-Stokes waves of FWM and MI effects. As a result, the expected continuum spectrum below 1550nm does not obviously appear.

4.1.2 Performance and comparison with other CW pumped OSC

Spectrum coverage

The 20dB bandwidth of the OSC in this experiment is 350nm, from 1550nm to 1900nm. To our best knowledge, this is the first CW pumped OSC which generates continuum spectrum above 1750nm. Before this OSC source, there are only two ultrashort pulse pumped OSCs have been reported to exceed 1750nm [25, 39]. The upper-limit wavelength in one case is 2500nm [39] and 1800nm in another [25]. As mentioned in the previous section, the wide spectrum coverage at long-wavelength region is benefited from the cascaded SRS effect generated by second peak. Thus, the result also proves SRS effect is the essential nonlinear effect to broaden spectrum in our case.

It should be noted that the high loss of fiber coupler decreases the power of high-order SRS Stokes peak, thus suppressing the generation of cascaded SRS Stokes peaks. As a result, the spectrum broadening toward long-wavelength region is limited. This suggests a possibility of further increasing the spectrum coverage by replacing current fiber coupler with a wideband fiber coupler. However, the problem caused by band-limited fiber coupler can be solved completely even using a wideband coupler.

Comparing to other CW pumped OSCs, although we can generate continuum spectrum at longer wavelengths, our OSC has a poor spectrum broadening below 1550nm. As discussed in Section 4.1.1, the problem is caused by intense SRS effect. The wide coverage at long-wavelength region is contributed by the intense SRS effect.

However, the intense SRS effect suppresses the spectrum broadening toward the short-wavelength direction.

This problem that SRS effect suppresses short-wavelength spectrum broadening could be solved by increasing the pump power more. Figure 4-1 which shows the spectra before OSC is formed and after OSC is formed, it can be found that the spectrum broaden toward short wavelength a little. Thus, it is inferred that the spectrum broadening toward short wavelength direction can be obtained by increasing the pump power further. However, we cannot prove it, since the devices in this OSC source would be damaged if the pump power was increased more.

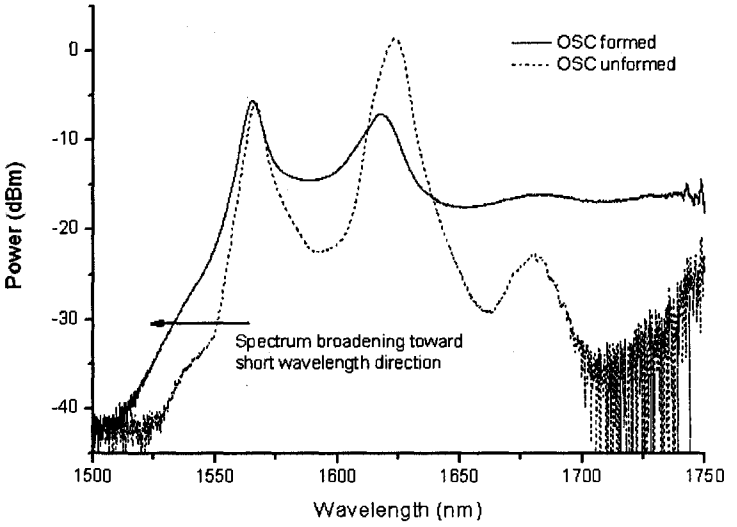

Figure 4-1 Spectrum broadening toward short-wavelength direction.

Flatness of spectrum

From Figure 3-12, we can find that the spectrum of our OSC is relatively smooth and flat at most regions, except for the spectral peaks of seed beam and the second

beam. A major reason that relatively flat and smooth OSC is generated is because intense SRS effect reduces the intensity of MI effect, thereby reducing the MI induced spectral vibration. As mentioned in Chapter one, the evolution mechanism where MI and SRS dominate CW pumped OSC generation is accepted by most researchers and was observed in most of experiment of CW pumped OSC. However, a problem in this mechanism is that MI effect could cause spectral vibration which will reduce the performance of OSC source. Figure 4-2 shows a MI and SRS dominated CW pumped OSC which is obtained in an experiment conducted by S. M. Kobtsev, et al., [32]. In this figure, we can find MI and MI induced soliton effect causes intense spectral vibration. In our OSC, SPM and SRS dominate the evolution, instead of MI and SRS dominated this process. Thus, by comparing the two results of Figure 3-12 and Figure 3-16, it is can be concluded that the OSC evolution dominated by SPM and SRS effects has the advantage on generating high performance OSC.

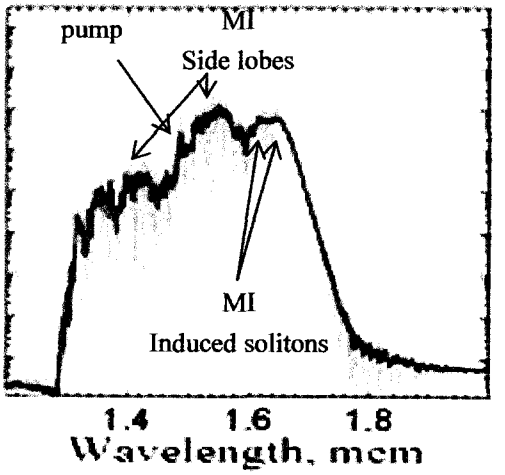

Figure 4-2 MI and SRS dominated CW pumped OSC (source [32])

Additionally, it is possible that the FWM also contributes to the flatness of

spectrum. The fact that FWM causes the spectrum between the SRS peak and the second peak to be flat can be observed in the evolution (Figure 3-12). It is inferred that SPM induced phase matching could induce FWM effect to occur at further wavelengths away from the seed peak. These new frequency components generated by FWM fall in the Raman gain spectrum and are amplified by Raman gain. As a result, a local uniform spectrum is formed the SRS peak and the second peak.

4.2 Conclusions

CW pumped OSC source, as a new type of OSC source, has been studied in recent years. In this experiment, a low-cost CW pumped OSC source is proposed. This OSC source is based on an Erbium/Ytterbium co-doped fiber ring cavity laser which allows the source to use shorter nonlinear fiber or lower pump power than those in other CW pumped OSC sources. The OSC is obtained using an HNLF that is several times shorter than those in other CW pumped OSC studies when pump power is 5.35W.

The output spectrum of the OSC source has 350nm coverage, from 1550nm to 1900nm. To our knowledge, this is the first CW pumped OSC source that generates supercontinuum spectrum above 1750nm wavelength. This infrared supercontinuum has multiple applications, such as optical communication, spectroscopy, and biotechnology. The wide spectrum coverage at long wavelength is benefited from the SRS effect which generates multiple Stokes peaks, broadening the spectrum to about 1900nm. However, since one of the experiment devices, fiber coupler, has a high

insertion loss at long wavelengths, the SRS effect is suppressed. As a result, the OSC spectrum cannot be extended toward longer wavelength than 1900nm.

Furthermore, the mechanism of this OSC evolution is analyzed. The analysis of the results shows that SPM and SRS dominate the evolution of OSC. The evolution pattern is different from the patterns of other CW pumped OSCs where the MI and SRS effects, or purely SRS effect contribute dominantly OSC generation. In this work, SPM dominates the spectral broadening and SRS are responsible for the broadening toward long-wavelength region. Also, the final OSC shows that the spectrum generated with this evolution pattern has high flatness. Two reasons contribute to the flat spectrum. Firstly, SPM induced spectrum broadening produces smooth spectrum. Secondly, the intense SRS effect suppresses the MI effect, thus avoiding the MI induced spectral vibration. The intense SPM and SRS effects are benefited from the ring-cavity structure which effectively increases the effective length of the nonlinear fiber.

4.3 Future works

The coverage of the OSC spectrum in our experiment is limited by the fiber coupler, which has high loss at long wavelengths. This problem cannot be easily solved because almost all attainable fiber couplers have high loss at long wavelengths. Future studies could focus on finding a broad band alternative of the fiber coupler in order to further increase the spectral coverage.

In this work, although the OSC spectrum was not extended toward short wavelength

region, since the SRS reduces the intensity of MI and FWM at short-wavelength side of the seed beam, current experiment setup still can be used to generate OSC at short wavelengths. If the pump power was increased further, the MI effect could be enhanced to generate OSC spectrum at short wavelengths. However, the optical devices in this experiment should be replaced with those which have higher handling power. Two other methods could also solve this problem. The first one is to use dispersion flatten fiber to enhance MI effect. The dispersion flatten fiber has low dispersion over a wide spectral range. Thus, the MI effect can be enhanced due to the low dispersion. The other is to scramble the polarization of pump beam in order to increase the threshold power of SRS, thus decreasing its suppressing effect on MI by increasing the requirement for generating SRS.

Reference

1. John M. Dudley and Stéphane Coen, "Coherence properties of supercontinuum spectra generated in photonic crystal and tapered optical fibers", *Optics Letters, Vol. 27, No. 13, pp: 1180-1182; 2002.*
2. Taccheo. S, Ennser. K, Forin. D, Tosi-Beleffi. G, Curti. F, "Supercontinuum-based devices for telecom applications", *Transparent Optical Networks 2006 International Conference, Vol 1, pp: 32 - 36; 2006.*
3. T. Nakasyotani, T. Kuri, H. Toda and K.-I. Kitayama, "Characterizations of supercontinuum light source for WDM millimeter-wave-band radio-on-fiber systems", *Photonics Technology Letters, Vol 17, No. 6, pp: 1274 - 1276; 2005.*
4. T. Morioka, K. Mori, S. Kawanishi and M. Saruwatari, "Multi-WDM-channel, Gbit/s pulse generation from a single laser source utilizing LD-pumped supercontinuum in optical fibers", *Photonics Technology Letters, Vol. 6, No. 5, pp: 365-367; 1994.*
5. H. Takara, T. Ohara, T. Yamamoto, H. Masuda, M. Abe, H. Takahashi and T. Morioka, "Field demonstration of over 1000-channel DWDM transmission with supercontinuum multi-carrier source", *Electronics Letters, Vol. 41, No. 5, pp: 270 - 271; 2005.*
6. C.-S. Brès, I. Glesk and P. R. Prucnal, "Demonstration of an eight-user 115-Gchip/s incoherent OCDMA system using supercontinuum generation and optical time gating", *Photonics Technology Letters, Vol. 18, No. 7, pp: 889-891; 2006.*
7. S. Moon and D. Y. Kim, "Ultra-high-speed optical coherence tomography with a stretched pulse supercontinuum source", *Optics Express, Vol. 14, No. 24, pp: 11575-11584; 2006.*
8. M. E. Staymates, G. S. Settles, K. Shi and Z. Liu, "Supercontinuum laser illumination applied to traditional optical flow imaging methods", *Optics Communications, Vol. 273, No. 1, pp: 252-255; 2007.*
9. X. Ni, C. Wang, X. Liang, M. AL-Rubaiee and R. R. Alfano, "Fresnel diffraction supercontinuum generation", *IEEE Journal of Selected Topics in Quantum Electronics, Vol 10,*

No. 5, pp:1229 - 1232; 2004.

10. G. P. Agrawal, "Nonlinear fiber optics", *Third Edition, Academic Press, Inc., 2001.*
11. G. P. Agrawal, "Fiber-optic communication system", *Third Edition, John Wiley & Sons, Inc., 2002.*
12. H. Sone, T. Kawano, M. Imai and Y. Imai, "Numerical analysis of supercontinuum generation in a dispersion flattened/decreasing fiber", *IEEE Communications 1999, Fifth Asia-Pacific Conference, Vol. 1, pp: 357 - 360; 1999.*
13. R. R. Alfano and S. L. Shapiro, "Emission in the region 4000 to 7000 Å via four-photon coupling in glass", *Physical Review Letters, Vol. 24, pp: 584-586; 1970.*
14. R. R. Alfano and S. L. Shapiro, "Observation of self-phase modulation and small-scale filaments in crystals and glasses", *Physical Review Letters, Vol. 24, pp: 592-595; 1970.*
15. C. Vinegoni, M. Wegmuller and N. Gisin, "Measurements of the nonlinear coefficient of standard SMF, DSF, and DCF fibers using a self-aligned interferometer and a faraday mirror", *Photonics Technology Letters, Vol. 13, No. 12, pp: 1337 - 133; 2001.*
16. W. J. Wadsworth, N. Y. Joly, F. Biancalana, J. C. Knight, T. A. Birks and P. S. J. Russell, "Compact supercontinuum generation and four-wave mixing in PCF with 10 ns laser pulses", *Conference on Lasers and Electro-Optics (CLEO) 2004, Vol. 2, No. 2, pp: 16-21; 2004.*
17. K. K. Chow, Y. Takushima, C. Lin, C. Shu and A. Bjarklev, "Flat supercontinuum generation in a dispersion-flattened nonlinear photonic crystal fiber with normal dispersion", *Optical Fiber Communication Conference (OFC) 2006, Technical Digest (CD) (Optical Society of America, 2006), paper OFH5; 2006.*
18. T. Okuno, M. Onishi and M. Nishimura, "Dispersion-flattened and decreasing fiber for ultra-broadband supercontinuum generation", *IEEE Integrated Optics and Optical Fibre Communications, 11th International Conference, Vol. 5, pp: 77 - 80; 1997.*
19. T. Yamamoto, H. Kubota, S. Kawanishi, M. Tanaka and S. Yamaguchi, "Supercontinuum generation at 1.55 nm in a dispersion-flattened polarization-maintaining photonic crystal fiber", *Optics Express, Vol. 11, No. 13, pp: 1537-1540; 2003.*

20. A. Demircan and U. Bandelow,"Impact of modulation instability on the supercontinuum generation", *IEEE Numerical Simulation of Optoelectronic Devices conference 2005, pp: 65-66; 2005.*

21. A. Kudlinski, A. K. George, J. C. Knight, J. C. Travers, A. B. Rulkov, S. V. Popov and J. R. Taylor, "Zero-dispersion wavelength decreasing photonic crystal fibers for ultraviolet-extended supercontinuum generation", *Optics Express, Vol. 14, No. 12, pp:5715-5722; 2006.*

22. G. Genty, M. Lehtonen and H. Ludvigsen, "Effect of cross-phase modulation on supercontinuum generated in microstructured fibers with sub-30 fs pulses", *Optics Express, Vol. 12, No. 19, pp: 4614-4624; 2004.*

23. T. Schreiber, T. Andersen, D. Schimpf, J. Limpert and A. Tünnermann, "Supercontinuum generation by femtosecond single and dual wavelength pumping in photonic crystal fibers with two zero dispersion wavelengths", *Optics Express, Vol. 13, No. 23, pp: 9556-9569; 2005.*

24. K. L. Corwin, N. R. Newbury, J. M. Dudley, S. Coen, S. A. Diddams, B. R. Washburn, K. Weber and R. S. Windeler, "Fundamental amplitude noise limitations to supercontinuum spectra generated in a microstructured fiber", *Applied Physics B, Vol. 77, No. 2, pp: 269-277; 2003.*

25. J. T. Gopinath, H. M. Shen, H. Sotobayashi, E. P. Ippen, T. Hasegawa, T. Nagashima and N. Sugimoto, "Highly nonlinear bismuth-oxide fiber for supercontinuum generation and femtosecond pulse compression", *Lightwave Technology, Vol. 23, No. 11, pp:3591 - 3596; 2005.*

26. K. Saitoh and M. Koshiba, "Highly nonlinear dispersion-flattened photonic crystal fibers for supercontinuum generation in a telecommunication window", *Optics Express, Vol. 12, No. 10, pp: 2027-2032; 2004.*

27. V. C. V. Tombelaine, P. Leproux, L. Grossard, J. -L. Auguste, and J. -M. Blondy, "Modulational instabilities in normal dispersion region leading to white-light supercontinuum generation", *Photonics Technology Letters, Vol. 14, No. 3, pp: 137 - 139; 2003.*

28. P.-A. Champert, V. Couderc, P. Leproux, S. Février, V. Tombelaine, L. Labonté, P. Roy, C. Froehly and P. Nérin, "White-light supercontinuum generation in normally dispersive optical fiber using original multi-wavelength pumping system", *Optics Express, Vol. 12, No. 19, pp:*

4366-4371; 2004.

29. K. P. Hansen and R. E. Kristiansen, "Supercontinuum generation in photonic crystal fibers," *IEEE Lasers and Electro-Optics 2005, (CLEO), Vol. 2, No. 3, pp: 1255-1257; 2005.*

30. A. K. Abeeluck, S. Radic, K. Brar, J.-C. Bouteiller and C. Headley, "Supercontinuum generation in a highly nonlinear fiber using a continuous wave pump", *Optical Fiber Communication Conference (OFC) 2003, Technical Digest (Optical Society of America, 2003), paper ThT1; 2003.*

31. A. V. Avdokhin, S. V. Popov and J. R. Taylor, "Continuous-wave, high-power, Raman continuum generation in holey fibers", *Optics Letters, Vol. 28, No. 15, pp: 1353~1355; 2003.*

32. S. M. Kobtsev and S. V. Smirnov, "Modelling of high-power supercontinuum generation in highly nonlinear, dispersion shifted fibers at CW pump," *Optics Express, Vol. 13, No. 18, pp: 6912-6918; 2005.*

33. A. K. Abeeluck and C. Headley, "Continuous-wave pumping in the anomalous- and normal-dispersion regions of nonlinear fibers for supercontinuum generation", *Optics Letters, Vol. 30, No. 1, pp: 61-63; 2005.*

34. A. K. Abeeluck and C. Headley, "High-power supercontinuum generation in highly nonlinear, dispersion-shifted fibers by use of a continuous-wave Raman fiber laser", *Optics Letters, Vol. 29, No. 18, pp: 2163~2165; 2004.*

35. T. Sylvestre, A. Vedadi, H. Maillotte, F. Vanholsbeeck and S. Coen, "Supercontinuum generation using continuous-wave multiwavelength pumping and dispersion management", *Optics Letters, Vol. 31, No. 13, pp:2036-2038; 2006.*

36. J. H. Lee, Y.-G. Han and S. Lee, "Experimental study on seed light source coherence dependence of continuous-wave supercontinuum performance", *Optics Express, Vol. 14, No. 8, pp: 3443-3452; 2006.*

37. J. C. Travers, S. V. Popov, J. R. Taylor, H. Sabert and B. Mangan, "Extended bandwidth CW-pumped infra-red supercontinuum generation in low water-loss PCF", *Conference on Lasers and Electro-Optics (CLEO) 2005, Technical Digest (CD) (Optical Society of America, 2005),*

paper CFO4; 2005.

38. S. Li, A. B. Ruffin and D. V.Kuksenkov, "Efficient generation of CW supercontinuum in optical fiber pumped by ASE light", *Optical Fiber Communication Conference (OFC) 2006, Technical Digest (CD) (Optical Society of America, 2006), paper OWI32; 2006.*
39. J. Takayanagi, N. Nishizawa, H. Nagai, M. Yoshida and T. Goto, "Generation of high-power femtosecond pulse and octave-spanning ultrabroad supercontinuum using all-fiber system", *Photonics Technology Letters, Vol. 17, No. 1, pp: 37 - 39; 2005.*
40. B.-C. Hwang, S. Jiang, T. Luo, J. Watson, G. Sorbello and N. Peyghambarian, "Cooperative upconversion and energy transfer of new high Er^{3+}- and Yb^{3+}-Er^{3+}-doped phosphate glasses", *Optical Society of America B, Vol. 17, No. 5, pp:833-839; 2000.*
41. J. N. Kutz, C. Lynga and B. J. Eggleton, "Enhanced supercontinuum generation through dispersion-management", *Optics Express, Vol. 13, No. 11, pp: 3989-3992; 2005.*
42. Lee.J.H., Kim.C.H., Han.Y.-G. and Lee.S.B., "Broadband, high power, erbium fibre ASE-based CW supercontinuum source for spectrum-sliced WDM PON applications," *Electronics Letters, Vol. 42, No. 9, pp:549 - 550; 2006.*
43. S. Kaasalainen, T. Lindroos and J. Hyyppä, "Toward hyperspectral lidar: measurement of spectral backscatter intensity with a supercontinuum laser source", *Geoscience and Remote Sensing Letters, Vol. 4, No. 2, pp: 211-215; 2007.*
44. H. Kano and H.-o. Hamaguchi, "In-vivo multi-nonlinear optical imaging of a living cell using a supercontinuum light source generated from a photonic crystal fiber", *Optics Express, Vol. 14, No. 7, pp: 2798-2804; 2006.*
45. T. Schreiber, J. Limpert, H. Zellmer and A. Tunnermann, "5 W supercontinuum based on an ultrafast fiber system", *Lasers and Electro-Optics Europe, 2003 (CLEO), pp: 249-252; 2003.*
46. Ju Han Lee, Kazuhiro Katoh and Kazuro Kikuchi, "Experimental investigation of continuous-wave supercontinuum ring laser composed of clad-pumped Er/Yb codoped fiber and highly-nonlinear optical fiber", *Optics Communications, Vol. 266, No. 2, pp: 681-685; 2006.*